SINGLE PALLADIUM NANOWIRE: SYNTHESIS VIA ELECTROPHORESIS DEPOSITION AND HYDROGEN SENSING

by

Yushi Hu

B.S. in Microelectronics Engineering, Fudan University, China, 2006

Submitted to the Graduate Faculty of

the Swanson School of Engineering in partial fulfillment

of the requirements for the degree of

Master of Science

University of Pittsburgh

2008

UNIVERSITY OF PITTSBURGH

SWANSON SCHOOL OF ENGINEERING

This thesis was presented

by

Yushi Hu

It was defended on

July 23, 2008

and approved by

Dr. Joel Falk, Professor, Department of Electrical and Computer Engineering

Dr. Kevin Chen, Associate Professor, Department of Electrical and Computer Engineering

Dr. Minhee Yun, Assistant Professor, Department of Electrical and Computer Engineering

Thesis Advisor: Dr. Minhee Yun, Department of Electrical and Computer Engineering

SINGLE PALLADIUM NANOWIRE: SYNTHESIS VIA ELECTROPHORESIS DEPOSITION AND HYDROGEN SENSING

Yushi Hu, M.S.

University of Pittsburgh, 2008

Palladium (Pd) single nanowires with less than 100 nm thickness have been successfully and repeatedly fabricated using electrophoresis deposition method. This work also demonstrates the use of a single Pd nanowire as a hydrogen sensor with extremely high sensitivity. Growth and sensing mechanisms are discussed in detail and an improved synthesis method is proposed and proved.

Single Pd nanowires were electrodeposited within 100 nm wide Poly-Methyl-Methacrylate (PMMA) nanochannels by using a probe station. The PMMA channels were fabricated by Electron Beam Lithography (EBL) on a pre-patterned template fabricated via photolithography and lift-off processes. Through this method, nanowires were grown with widths ranging from 50 nm to 100 nm, and lengths from 3.5 μm to 6.5 μm. The nanowires, successfully integrated into hydrogen sensor devices, were able to sense hydrogen concentrations as low as 5 ppm (part per million) at room temperature. Three different nanowire structures were found, and the growth control of nanowire structure was conducted. Different sensing mechanisms were addressed in detail according to different nanowire structures.

A newly developed gate assisted growth method were also proposed and demonstrated in this work. Thinner and more uniform nanowires were synthesized with this method, and the growth time was greatly reduced. Experimental data were presented to approve the effects of gate voltage on nanowire diameter and growth time.

TABLE OF CONTENTS

LIST OF TABLES

LIST OF FIGURES

PREFACE

I first thank my advisor, Dr. Minhee Yun. Without his relentless support, instruction, patience, and advice, I could never have done this work. Even more importantly, his enthusiasm in innovations, attitude towards research and optimism deeply impressed and encouraged me. I am grateful to Dr. Yun on a professional and personal level.

I also thank Professor Joel Falk and Professor Kevin Chen for joining my committee and giving me precious advice on my thesis. I further thank my fellow researchers, Dave Perello, Innam Lee, Usman Mushtaq, and Dr. Hoil Park, for their continuous support.

Finally, I thank my parents for giving me the opportunity experience an intensive education, and my girlfriend for her constant care and support.

1.0 INTRODUCTION

1.1 MOTIVATION

The sensors industry has been considered one of the most important industries in the world. A great deal of research has focused on ways to fabricate small, highly sensitive and energy efficient sensors [1]. Among countless chemical sensors, hydrogen gas sensor emerges as a special yet promising one. The hydrogen gas sensors are used widely in the gas storage and fabrication industry for monitoring hydrogen concentration with security purposes. An increased demand for faster and higher sensitive monitors emerges along with the development of aerospace techniques and hydrogen fuel cell industry [2, 3]. Also, energy efficiency issues arise with the development of green house and environment sustainability. Hydrogen sensors with a smaller size, better performance, easier fabrication, and lower energy consumption have a potentially large market [4].

Many researchers have focused on fabricating different hydrogen sensors, which can be categorized into pyroelectric sensors, piezoelectric sensors, fiber optic sensors (FOS), electrochemical sensors, and semiconductor (FET) sensors [5]. Within these sensors, a very high sensitivity has been obtained by using the Pd-FET structure or FET structure coated with other catalytic materials (Pt for example) and these structures are believed to be superior to other non-FET sensors. However, they usually suffer from a high operation temperature and a more

complicated fabrication process [5]. New hydrogen sensors based on non-FET structures with easy fabrication process and room temperature operation are needed.

The nanowire based hydrogen sensor is a very promising candidate in this regard. Nanowires, either semi-conducting or metallic, have long attracted a great deal of attention because of their unique properties [6]. Researchers have proposed nanosized structures or devices with new and/or enhanced functions based on nanowires, such as field effect transistors based on semiconductor nanowires [7], light emitting diode [8], biosensors [9], chemical sensors [10], and thermocouples [11]. Defined as a one-dimensional (1D) structure, a nanowire often refers to a wire with a diameter under 100nm and aspect ratio (length to width ratio) as large as 1000 [12]. Because of their small diameter, nanowires have a much larger surface to volume ratio than thin films which are used in conventional FET or FOS structures. Higher surface could facilitate higher sensitivity when sensing is based on surface interaction between catalytic materials and sensing targets. This makes nanowire based nanosensors a powerful and general class of ultrasensitive, electrical sensors for the direct detection of biological and chemical species [13].

Hydrogen gas sensors based on metallic nanowire arrays [14] or bundles [15] have been reported by multiple groups; these sensors excel in sensitivity or response time compared to conventional non-FET sensors. They also show an advantage in easy fabrication since they are based on pure Pd nanowires and, therefore, avoid the complicated process required by FET sensors. However, they are still not comparable to FET sensors in sensitivity. A closer look reveals that nanowire arrays or bundles are still based on the overall performance of a collection of individual nanowires; this might undermine the advantages that an individual nanowire might have. A single nanowire structure, which demonstrates a truly 1D structure, indicates higher

research value since the individual nanowire is being researched directly. Single nanowire hydrogen gas sensors, taking full advantage of high surface to volume ratio, show great potential in achieving higher sensitivity than arrays or bundles.

In spite of its advantage, the single nanowire device has always been difficult to fabricate or align. Vapor-Liquid-Solid growth has been demonstrated as an effective fabrication method for semiconductor nanowires, especially Si nanowire [7]. However, this process does require high temperature or catalysts during the process. Chemical Vapor deposition (CVD), also reported for nanowire growth, needs a complex fabrication process [16]. Besides, the alignment of single nanowire should be addressed. As a controllable and feasible growth method, electrochemical deposition could avoid these problems. By using a proper electrolyte solution, Pd nanowire growth can be finished within a probe station at room temperature within minutes. Meanwhile, the nanowire is self-aligned and connected to the electrodes, thereby avoiding the alignment process [17].

Motivated by the above advantages, in this work Pd single nanowires are grown using electrochemical deposition and hydrogen sensors are integrated based on them. Sensors with high sensitivity, low power consumption, small size, and easy fabrication process are expected. Additionally, the response of single nanowire to hydrogen and the idea that single nanowire has advantage over traditional thin film or nanowire arrays are investigated. Finally, an entirely new idea of electrodepositing nanowires with multiple electric fields is proposed and demonstrated.

1.2 THESIS ORGANIZATION

Chapter 2 introduces the background information of this thesis. It presents the general ideas of the one-dimensional structure and the advantages of nanowires. The properties of metallic nanowires, especially conductance, and fabrication techniques are included. The key fabrication processes, such as electrophoresis deposition and Electron-Beam Lithography, are fully addressed. Palladium properties and hydrogen palladium interactions are also discussed.

Chapter 3 covers the experimental details of this work, including the complete template fabrication process, electrophoresis deposition of the nanowire in probe station, sensor device preparation and integration into the gas sensing system, and the set up of the gas sensing data acquisition system.

Chapter 4 deals with the results and data from experiments with detailed analysis. The growth of different nanowire structures and the control of nanowire structure are presented and discussed. Hydrogen sensing signal and sensor performance are analyzed in detail, while the relationship between the nanowire structures and the sensing mechanisms are presented. An entirely new approach of gate voltage assisted nanowire growth is proposed and proved.

Chapter 5 draws the conclusions and summarizes the accomplishments of this work. The potential of our research in biosensing area and possible future steps are included.

2.0 BACKGROUND

2.1 ONE DIMENSIONAL NANOSTRUCTURE AND NANOWIRE

Dimensionality of substances, such as bulk materials, thin films, wires, and small particles, is defined by the directions of high conductivity, or electron flow, in the material. In a three dimensional or 3-D structure (Figure 2.1.1A), such as a gold brick, electrons flow freely in all directions (x, y, z). However, in a two dimensional or 2-D structure (Figure 2.1.1B), such as aluminum foil, electron flows are restricted in a plane (x-y plane). In a one dimensional or 1-D structure (Figure 2.1.1C), such as a carbon nanotube, electrons can only flow in one direction along the nanotube (y direction) but are very restricted in other directions (x, z). In a zero dimensional structure, such as a gold nanoparticle, the electrons are limited inside the boundary of a particle with zero direction to flow.

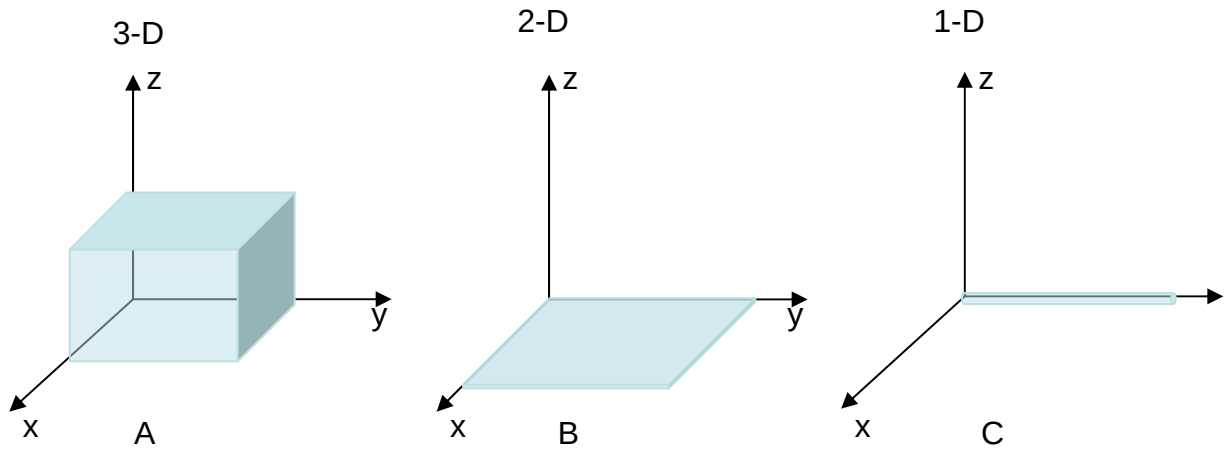

Figure 2.1.1 Illustration of (A) 3D, (B) 2D, and (C) 1D structures.

Experimental studies of 1-D electronic systems could date back to the beginning of the 1970s when it first became possible to synthesize 1-D conductors [18]. Early research on 1-D

structures were initiated with the hope of realizing high temperature superconductors. While the quest for high temperature superconductors has not been fulfilled in the past 40 years, the interest in 1-D structures has never faded, especially when technology goes into nanometer range. 1-D nanostructures, such as wires, belts, and tubes, are often referred to as those with lateral dimensions that fall in the range of 1nm to 100nm. 1-D nanostructures have several advantageous features:

The first feature is their small size. As predicted by Moore's Law, the feature size of Integrated Circuit devices is halved every 18 months. In the microelectronics area, a smaller size means a higher device density, more functions, and better performance. With a lateral size smaller than 100 nm, 1-D nanostructures might replace the conventional FET structures based on bulk materials. FET structures based on semi-conducting nanowires, such as Si nanowires, have been demonstrated by numerous reports [7, 19]. Moreover, 1-D nanostructures might also be used as interconnect within CMOS structures. A field-programmable nanowire interconnect have been proposed and facilitated in a nano CMOS architecture [20]. In addition to microelectronics, 1-D nanostructures could also be used in bio-molecular or bio-medical area where small size of devices is a crucial issue.

Secondly, 1-D nanostructures are easily affected or confined by surface changes, such as attachment of surface charges or change of chemical states, which makes them extremely suitable for sensing purposes. For example, the effect of surface change in semi-conducting oxides will become prominent when the effective diameter of the nanostructure becomes comparable to the oxide's Debye screening length [9]. In such nanostructures, a tiny change in the chemical state of the surface due to the presence of chemical or biological agents can result in the redistribution (depletion or accumulation) of electrons not only at near surface but also in

the entire volume of the nanostructure. This depletion (or accumulation), which will result in a nontrivial signal that can be detected, thus enables the utilization of 1-D nanostructures as sensors.

Thirdly, 1-D nanostructures have a large surface to volume ratio; this again proves that they are very promising in sensors area. It can be easily substantiated that 1-D nanostructures have the largest surface to volume ratio among 3-D, 2-D, and 1-D structures. In a block with three dimensions of a, b, and c respectively, it can easily be calculated that the surface to volume ratio in this case is:

$$Surface\ to\ Volume\ Ratio\colon\ SVR = \ 2(ab + bc + ac)/abc \qquad (2.1)$$

In 3-D structures, a, b, and c are big and comparable to each other. Therefore equation (2.1) can be simplified as:

$$SVR(3D) = 2\ (1/c + 1/b + 1/a), \qquad a{\sim}b{\sim}c \qquad (2.2)$$

In 2-D structures, a and b are big, but c is much smaller than a or b. Equation (2.1) then becomes:

$$SVR(2D) \approx 2\ 1/c, \qquad a{\sim}b \gg c \qquad (2.3)$$

In 1-D structures, a is big, and b and c are much smaller than a. Equation (2.1) becomes:

$$SVR(1D) \approx 2(1/c + 1/b)\ , \qquad a \gg b{\sim}c \qquad (2.4)$$

It is clear that $SVR(1D) > SVR(2D) \gg SVR(3D)$. It is also clear from equation (2.4) that the surface to volume ratio is going to increase as the lateral dimensions decrease. With the largest surface to volume ratio among the three, 1-D nanostructures provide most surface reactive sites within certain volume, thus providing the best sensitivity.

Lastly, 1-D nanostructures exhibit many unique electrical and optical properties which, by providing fundamental understanding of physics in nanometer range, deserve an in-depth investigation. Electron transport in 1-D nanostructures is always an interesting issue. When the

diameter of 1-D nanostructures approaches the mean free path of electrons, the quantum effect of electron transportation is expected to take place. Researchers have conducted many studies in order to determine the quantum conductance of metallic nanowires; these studies have yielded interesting results [21]. Photoluminescence in 1-D nanostructures, such as Carbon Nanotubes (CNTs) and silicon or other semiconducting nanowires (NWs), and its potential use as Light Emitting Diodes (LEDs), is another issue under intense investigation. In addition, free-standing semiconducting nanowires can also act as stand-alone optical waveguides, cavities, and gain medium to support laser emission [22].

2.2 METALLIC NANOWIRE: PROPERTIES AND SYNTHESIS

Semiconducting nanowires, such as silicon nanowires, germanium nanowires, and GaAs nanowires, have been thoroughly investigated thoroughly because of their better compatibility with today's microelectronics industry and their potential in replacing conventional FET structures [7]. In addition, the properties of semiconducting nanowires or organic nanowires, such as easier surface modification and tunable sensitivity presented in FET structures, make them perfect candidates in the area of bio-sensors. Metallic nanowires, on the other hand, are explored primarily for their fundamental physical properties, such as quantum conductance [23], phase change and superconductivity [24]. Very few studies focus on their usage as nano devices such as sensors because of the lack of an easy and efficient fabrication method. The following subsection discusses some basic physical properties of nanowire conductance; this second part also includes fabrication techniques for metallic nanowires.

2.2.1 Electrical Properties

Metallic nanowire conductance has been a research focus for many years. Researchers have tried hard to discover how the conductance changes along with the diameter of nanowires. It is generally accepted that when the diameter of the nanowires approaches the mean free path of the electrons inside the nanowires, the electron transport should conform to the size dependent quantum effects [21]. Rather than the general expression of conductance:

$$G = \sigma A/L, \tag{2.5}$$

in which G represents the conductance, σ represents conductivity, A represents the area and L represents the length of the sample. Landauer's Formula offers a more accurate expression for conductance [21]:

$$G = (2e^2)/h\,T, \tag{2.6}$$

where e represents the electron charge, h represents the Plank constant, and T represents the transmission function that expresses the probability of transmitting an electron from one end of the conductor to the other end.

According to Eq. 2.6, by assuming the nanowire satisfies ballistic scattering for electrons we can draw a conclusion that the conductance of nanowire varies with its diameter. The conductance becomes smaller when the diameter is decreased and quantum conductance effect could happen when the diameter approaches the size of atoms. A complete explanation is included in the Appendix part.

2.2.2 Fabrication Techniques

How to grow nanowire arrays or bundles or single nanowires is always a critical part in nanowire related research. As mentioned above, semi-conducting and metallic nanowires have found their future applications in a wide range of areas, such as microelectronic circuits, chemical and bio sensors and superconductivity, etc. Scientists, engineers and other industry people now seek an efficient, economic, consistent, and easy to control technique of nanowire fabrication. While different research groups have proposed multiple methods for semi-conducting nanowire growth, including Laser Ablation [28], Chemical Vapor Deposition [29], and Self-Assembly [30], only a limited number of fabrication techniques are introduced for metallic nanowire. The synthesis techniques of metallic nanowire mainly fall into two categories: physical route and electrochemical deposition route.

2.2.2.1 Physical Route. Metallic nanowires have been successfully fabricated using physical methods without any chemical reactions, such as applying an electron beam bombardment on thin films and thinning the wire via electron beams. In order to study the quantization of nanowire conductance and the mechanical properties, thin wires down to a few angstroms could be made by stretching. Other physical processes, such as physical evaporation, have also been applied for conducting nanowire synthesis.

Forming a nanosized metallic nanowire using electron beam irradiation on thin films was explained in detail by Takayanagi [31, 32]. A gold (011) film of thickness 3–5 nm was used as the raw material. Electron beam irradiation was used to clean the film before putting the film under an intense electron beam (200 kV, 500 A/cm^2). A weaker electron beam (10–50 A/cm^2) was used for further thinning; new structures with diameters 0.6–1.5 nm and length 3–15 nm

were formed. High resolution tunneling electron microscopy revealed that the wires had a few atom rows [32].

Stretching a wire into an even smaller size by applying a tensile stress on both ends has been a commonly used method in fabricating nanowires with diameters of a few nanometers or even a few angstroms [33]. This method, based on the elasticity or mechanical properties of the material itself, can make a nanowire as thin as a few angstroms, depending on the specific material. However, the short length (less than a few nanometers) of this kind of nanowire limits the utilization of these nanowires in devices.

Physical evaporation is another technique for fabricating metallic or other conducting nanowires. Yanfa Yan et al. [34] reported metallic zinc nanowires synthesized by physical evaporation. They carried out the synthesis process in a quartz tube, using NH_3 as a carrier gas kept at a flow rate of 46 sccm (standard cubic centimeters per minute). The source material used to evaporate was pure ZnO powder mixed with graphite with a molar ratio of 1:1. The powder mixture was placed in a quartz crucible which was then inserted in the middle of the quartz tube. A horizontal tube furnace heated to 1100 °C was used as the growth chamber. A quartz plate was placed in the downstream end of the quartz tube. After 30 min evaporation, the quartz tube was taken out of the furnace and cooled to room temperature. Fluffy dark gray products were found on both the quartz plate and nearby areas on the inner wall of the quartz tube. SEM images showed that the as-deposited dark gray products consisted of a large quantity of nanowires with diameters from 20nm to 200nm [34].

2.2.2.2 Electrodeposition Route. Electrodeposition is the most efficient and practical way of metallic nanowire fabrication. Compared to other methods, it is relatively simple and inexpensive since it does not require a high temperature or high vacuum condition during

fabrication as physical deposition or e-beam thinning does. Metallic nanowires with excellent uniformity and surface properties have been synthesized and applied to multiple devices, such as chemical sensors and thermocouples. Electrodeposition of metallic nanowires is normally completed by using different templates, either natural porous structures or surfaces fabricated beforehand with the desired pattern. Three different kinds of templates - Anodic Aluminum Oxide (AAO), Highly Oriented Pyrolytic Graphite (HOPG), and trenches formed using lithography - are discussed below.

The anodic aluminum oxide (AAO) template is one of the most used templates in metallic nanowire fabrication. AAO films, which are grown in strong acid electrolytes, possess highly anisotropic porous structures with pore diameters ranging from below 10 to 200 nm and pore lengths from 1 to 50 μm. The pores are found to be uniform and nearly parallel with densities ranging from 10^9 to 10^{11} cm^{-2}; this makes the AAO films ideal templates for the electrochemical deposition of monodispersed nanometer scale particles [35]. Different metallic nanowires, such as CdS nanowires [35], Ni nanowires [36], and Palladium nanowires [15] have been successfully grown. SEM images of grown Pd nanowires prove the fairly uniform dispersion as well as uniform diameters of nanowires [15]. Despite its wide use, this method has several limitations. Since practical devices prefer lateral layout, nanowires grown in AAO, which are vertically distributed, have limited use in this area. Also, only nanowire bundles or arrays can be grown because of the structure of AAO; as a result, single nanowire cannot be synthesized.

A great deal of research on electrochemical deposited metallic nanowires has been based on highly oriented pyrolytic graphite (HOPG). Parallel arrays of metallic nanowires, such as Pd, have been successfully synthesized by using HOPG as a template [37]. Because of the layered structure, HOPG cleaves easily by pressing a tape on its surface and pulling it off. The freshly

cleaved surface consists of many parallel steps composed of several or dozens of atomic layers. Equally spaced parallel 'V' shaped grooves may also form on the surface of HOPG. During electrochemical deposition, metal ions prefer to sit at the step edges or 'V' grooves, thus forming arrays of parallel nanowires. MoO_2 nanowire arrays with a few microns in length and 40nm and 170 nm in diameter were presented in SEM images [38]. The nanowires fabricated in this way, which are quite uniform in diameter and highly oriented, can be used in practical devices, such as gas sensors. However, because of the structure of HOPG, it is still not possible to fabricate single nanowires in this way.

Despite of the easy availability of AAO or HOPG, there are limitations on the growth of nanowires, such as the orientation, density, and the diameter of the nanowires, because of the intrinsic structure of the template. In order to achieve better control of the nanowire growth, templates fabricated using lithography steps have been made. E.J. Menke *et al.* proposed a way of electrodepositing gold nanowires by patterning and then over etching Ni electrodes using optical lithography to grow nanowires in the trench formed by Ni and photoresist [39]. Since the electrodes are patterned by lithography, the growth of nanowires would conform to the pattern of the electrode, thereby controlling the growth of the nanowire. This method achieved the shape control of gold nanowires but suffered from a much more complicated process.

As discussed above, physical and electrochemical methods are the most used ones for metallic nanowire synthesis; the electrophoresis method seems to be the more promising and feasible approach. However, a great amount of research is still being conducted to explore ways to more efficiently and economically fabricate nanowires with desired morphology as well as physical and chemical properties.

2.3 BASICS OF ELECTROPHORESIS AND ELECTRODEPOSITION

Electrophoresis, the most known electrokinetic phenomenon, refers to the motion of dispersed particles relative to a fluid under the influence of an electric field that is space uniform. These particles carry a certain amount of surface charge so that the electric field inside the liquid exerts an electrostatic Coulomb force on the particles and drives positive particles toward anode and negative particles toward cathode. When a metallic salt is dissolved in water, it dissociates to form positively charged ions. The solution that contains these charged ions is referred to as an electrolye or a plating solution. Because of the existence of electrophoresis, positive charged metal ions drift toward cathode and attach to the surface when a sufficient amount of electric current is applied through this electrolyte. As a result, the metal ions can be reduced to form solid metal on the cathode end. This process is referred to as electrodeposition.

2.3.1 Water and Ionic solutions

The electrodeposition cell contains the following basic components: two metal electrodes (anode and cathode), water containing dissolved ions (electrolyte), and two metal-solution interfaces [40]. This cell can be illustrated as Figure 2.3.1. The components will be discussed in detail in the following sections.

The solution containing metal ions is the most important component of the electrodeposition system. Water is the medium used in solutions to provide an environment for the ions. Pure water is neutral in electrostatic charge with the same amount of H^+ and OH^- ions as a result of ionic dissociation [40]:

$$H_2O \leftrightarrow H^+ + OH^- \tag{2.17}$$

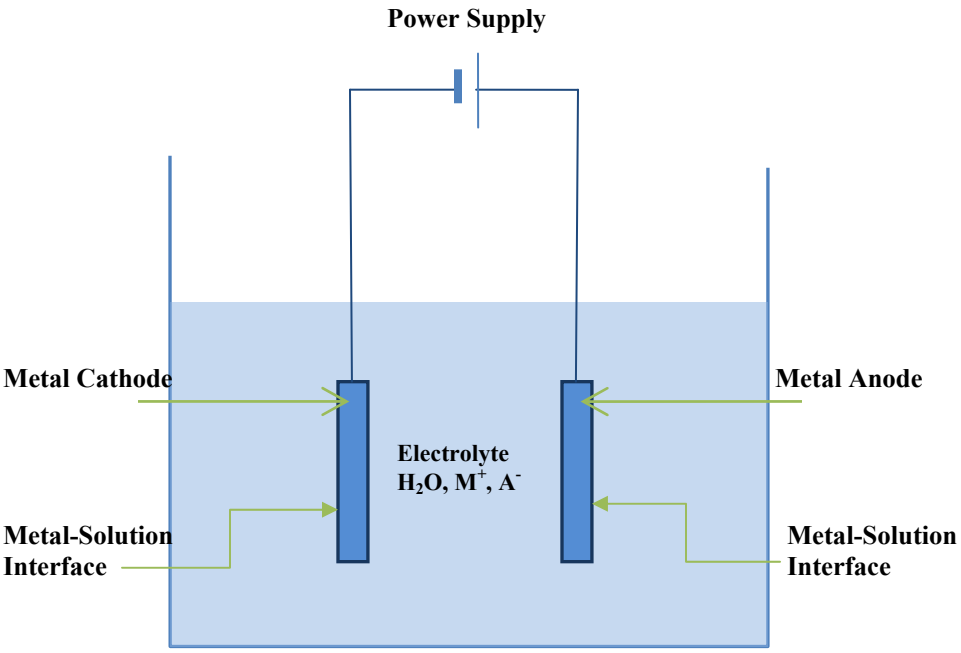

Figure 2.3.1 Illustration of a common electrodeposition cell configuration

This process is reversible and will reach a balance resulting in the same concentration of 1.0×10^{-14}mol/L for both H^+ and OH^- ions at 25°C. The ion-ion interaction in water is greatly affected by its dielectric constant. According to the Coulomb Law, the potential of electrostatic interaction U between two point charges q_1 and q_2 in a medium with dielectric constant ε is given by:

$$U = \pm(q_1 q_2)/\varepsilon r \tag{2.18}$$

Since the dielectric constant of water is 78.5, the electrostatic interaction is greatly reduced compared to that in a vacuum.

Two ways exists to form a solution by introducing ions in water. One method is by the dissolution of ionic crystal (e.g., NaCl) which is composed of separate positive (Na^+) and negative (Cl^-) ions. The overall dissolution process of an ionic crystal such as MA can be represented as [40]:

$$M^{z+}A^{z-} + (m+a)H_2O \rightarrow M^{z+}(mH_2O) + A^{z-}(aH_2O) \tag{2.19}$$

This process consists of two steps: (1) separation of ions from the ionic crystal lattice and (2) interaction of the ions with water molecules (hydration). Another method is the dissolution of a potential electrolyte such as HA in water. The process can be represented as [40]:

$$HA + H_2O \rightarrow H_3O^+ + A^- \tag{2.20}$$

The proton dissociated from the potential electrolyte HA (e.g. HOOCCOOH) will react with the water molecule and form a hydronium ion H_3O^-. The difference between these two methods lies in the fact that ionic crystals would form two separated ions while the latter forms hydronium ions instead of separated and chemically unstable protons. The commonly used electrolytes for metallic nanowire growth must fall in the first category since the positive ions are metallic ions instead of protons.

2.3.2 Mechanisms of Electrodeposition of Metals

During the process of electrodeposition of metals, metal ions (M^{n+}) in the solution are transferred into ionic metal lattices. The process can be represented as [40]:

$$M^{n+}(solution) \rightarrow M^{n+}(kink) \tag{2.21}$$

Since the metal ions in the solution are hydrated, as mentioned in the first case in section 2.3.1, M^{n+} should be replaced by $[M(H_2O)_x]^{n+}$. Considering the atomic structure of a metal surface, there exist different sites for the attachment of metal ions, such as terraces, step edges (ledges), and kink sites. Kink sites are most favorable because of their lowest energy state. Thus, metal ions would always like to sit at kink sites during their growth or deposition. As a result, equation (2.21) should be represented as [40]:

$$[M(H_2O)_x]^{n+}(solution) \rightarrow M^{n+}(kink) \tag{2.22}$$

And this process can be completed via two different mechanisms: (1) step-edge site ion transfer or (2) terrace site ion-transfer.

Step-edge site ion-transfer occurs when the ion-transfer proceeds at the kink sites or step-edge sites. In either case, the metal ion is transferred from the solution into the kink sites at the end. In the first case, the metal ions sit directly on the kink sites, while in the second case the metal ion is transferred to the step-edge and diffuses along the step-edge until it finds the kink sites. As a result, two possible paths for ion-transfer exist in step-edge site transfer: direct transfer to kink sites and the step-edge diffusion path. In this mechanism, the metal ion would lose half of its bonds with the water molecules but would bond with the metal surface. Thus, the ion belongs to the bulk crystal.

Terrace ion-transfer mechanism, on the other hand, happens when a metal ion is transferred from the solution into the flat face of the terrace region of the substrate surface. In this position, the metal ion has most of its water molecules and bonds weakly with the bulk crystal. But this position is not a stable one and the ion would diffuse on the surface seeking a lower energy position. The final site is a kink site.

Metal ions in the solution would transfer into the crystal and sit at the lowest energy sites - kink sites – either directly or through diffusion on the metal surface. These mechanisms formed the basis of our design for nanowire growth in which we purposely fabricated lower energy sites for metal ions deposition to confine the growth of the nanowire.

2.3.3 Nucleation and Growth Models of Electrodeposition

Nucleation and growth are the two steps involved in the electrodeposition of metals. Nucleation is the first step when initial nuclei sit on the surface of the substrate and form the basis of the further growth of metal crystals. This process is highly dependent on the surface structure of the substrate or, more specifically speaking, on how many nucleation sites exist on the substrate surface. The nucleation law for a uniform probability with time t of conversion of a site on the metal electrode into nuclei is given by [40]

$$N = N_0\big(1 - exp(-At)\big) \tag{2.23}$$

where N_0 is the total number of sites, and A is the nucleation rate constant. This equation represents the first-order kinetic model of nucleation. The rate of 2D nucleation J is given by [40]

$$J = k_1\, exp[-(bs\varepsilon^2)/zekT\eta] \tag{2.24}$$

where k_1 is the rate constant, b is the geometric factor depending on the shape of the 2D cluster, s is the area occupied by one atom on the surface of the cluster, ε is the specific energy, and k is

the Boltzmann constant. If the nucleation constant A is large, all electrode sites are instantaneously converted to nuclei. If A is small, the number of nuclei N is a function of time t, and the nucleation is progressive.

The growth of nuclei is another key step in electrodeposition. There are basically four simple models of nuclei: (a) a two-dimensional cylinder; (b) a three-dimensional hemisphere; (c) a right-circular cone; and (d) a truncated four-sided pyramid. The growth rate of a single 2 dimensional cylindrical nucleus and a single 3 dimensional hemispherical nucleus are given by [40]

$$i = \left(\frac{nFk^2 2\pi hM}{\rho}\right) t \tag{2.25}$$

and

$$i = \left(\frac{nFk^3 2\pi hM^2}{\rho^2}\right) t^2 \tag{2.26}$$

respectively, where i represents the growth current, k is the rate constant, h is the height of a nucleus, M is the molecular weight, and ρ is the density of deposit.

After the growth of a single nucleus, multiple nuclei might collide with each other, leading to the formation of a monolayer. There can be two different mechanisms: (1) the instantaneous nucleation mechanism according to which the monolayer is growing from the nuclei formed instantaneously on the substrate in t=0; and (2) the progressive nucleation mechanism in which nuclei appear randomly in space and time [40].

Once the monolayer is formed, the multilayer formation begins. There are two different mechanisms: (1) monolayer layer-by-layer growth and (2) multinuclear multilayer growth. The first mechanism happens when the overpotential applied is slightly higher than the critical overpotential and when the nucleation rate is slower than the growth rate of nucleus. In this case, each nucleus spreads over the entire surface before the next nucleus is formed. Therefore, the

growth occurs in a layer-by-layer mode. The second mechanism, however, happens at a higher overpotential when the nucleation rate greatly increases. Because the growth of each monolayer proceeds with the formation of many nuclei, this process is multinuclear.

A coherent deposit is formed after the completion of the growth of a number of monolayers. Layer growth and 3-D growth are the two mechanisms for the formation of coherent deposit. In the layer growth mechanism, a crystal grows by the lateral spreading of discrete layers one after another; each growth layer is a structure component. In 3-D growth mechanism, however, the coherent deposit is built by the coalescence of different 3-D crystallites which are the structure components in the deposit formed on substrate.

Different structures of deposit can be formed under different growth conditions, such as growth current or overpotential, which are directly related to the fact that the growth and nucleation process is dependent on the overpotential during growth. A correlation found by Seiter et al. between overpotential η and current density with corresponding growth forms of electrodeposited copper on copper sheet substrate presented this fact: four structural forms of copper: ridge, platelet, block, and polycrystalline existed and the higher the overpotential, the more disordered the deposit would be. Finer structure was formed under small overpotential.

2.4 E-BEAM LITHOGRAPHY AND PMMA

2.4.1 PMMA: Properties and Application as Resist

Polymethylmethacrylate, abbreviated as PMMA, is a thermoplastic and transparent plastic. Commonly referred to as acrylic glass, it is even clearer than normal glass and works as an alternative to glass in many areas. Its molecular formula is $(C_5O_2H_8)_n$ and its density is 1.19

g/cm³. It has a melting point of 130–140 °C and a spoiling point of 200.0 °C. Because PMMA's surface and volume resistivity are 10^{14} Ω/sq and $2-14\times10^{15}$ Ω·cm, respectively, it is an insulator. Although PMMA can be used for many imaging and non-imaging microelectronic applications, its most common use is as a high resolution positive resist for direct electron beam as well as X-ray and deep UV writing in microlithographic processes. Since PMMA has no sensitivity to white light, it is very suitable for clean room or even lab environment use. Sometimes, PMMA is also used as a protective coating for wafer thinning, such as a bonding adhesive, and as a sacrificial layer.

Standard PMMA resist products cover a wide range of film thicknesses and are formulated with 495,000 & 950,000 molecular weight (MW) resins in either chlorobenzene or the safer solvent anisole. Depending on the solvent type and the weight percentage, PMMA resist can be categorized as A2, A4, A6… C2, C4, C6… etc., "A" represents Anisole, "C" represents Chlorobenzene, and the numbers (2, 4, 6…) represent the weight percentage of PMMA in solution [41].

2.4.2 E-Beam Lithography: Fundamentals and Processes

Electron beam lithography, often abbreviated as e-beam lithography or EBL, is the process in which a patterned beam of electrons is scanned across a surface covered with a layer of resist (such as PMMA), and either exposed (i.e. positive resist, PMMA) or non-exposed (negative resist) regions of the resist are selectively removed. It is different from conventional photo lithography in that its source is no longer UV light but electron beams with a much smaller wavelength. A key advantage of e-beam lithography is that it is able to fabricate features within nanometer range because of its small wavelength and small diffraction effect. Theoretically, the

minimum feature size it can achieve is only a few nanometers, but because of the proximity effect, the resulted feature size is broadened. However, by using a proper process and resist, the fabrication of structures with an aspect ratio of 10 with widths less than 40 nm can be successfully done [42]. E-beam lithography is also more desirable for fabricating a specific pattern within the nanometer scale since it is a maskless and point-to-point process. However, EBL also suffers from long exposure time (~2hr/wafer) and low throughput.

The standard e-beam lithography process, including wafer cleaning, resist spin-on, pre-bake, e-beam writing, development, and post-bake, resembles that of photolithography. For PMMA resists, the post-bake is not necessary. Table 1 presents a recipe of a 100nm feature size e-beam lithography process developed in our experiment. With this recipe, we were able to fabricate channels with dimensions: 100 nm(Width)×150 nm(Depth)×30 μm(Length).

2.5 PALLADIUM AND HYDROGEN-PALLADIUM SYSTEM

Palladium (Pd) is perhaps the most commonly used material in today's applications related to hydrogen, such as hydrogen sensors and hydrogen storage. When it comes to the nanotechnology area, palladium thin films and mesowires or nanowires have been reported as effective hydrogen sensors or switches [43, 14]. In this thesis, we use Pd as the material to fabricate single nanowires and to study its response to hydrogen because of its unique properties.

2.5.1 General Properties of Palladium

Palladium is a soft silver-white metal that resembles platinum. Along with platinum, rhodium, ruthenium, iridium, and osmium, palladium belongs to a group of elements referred to as the

Table 1 A recipe for a 100 nm feature size E-Beam Lithography Process

Substrate preparation	
Substrate Cleaning	Acetone→Methanol→IPA→Dry N_2
Dehydration	Hotplate, 200°C, 5min
Resist Coating	
Resist	PMMA, A4
MCC Primer	Static Dispense, 3000rpm, 30sec
Dispense	Dynamic Dispense: 450rpm, 6sec
Spin	5000rpm, 1min
Prebake	170°C, in oven, 30min
Thickness	150nm
Exposure conditions	
Aperture	30μm
Step size	10nm
Working Distance	6mm
Write field	100μm×100μm
Acceleration Voltage	10kV
Resist Development	
Developer	MIBK:IPA=1:3
Time	15~20sec
Rinse and Dry	IPA, 20sec; Dry N_2
Postbake(optional)	100°C, 2min

platinum group metals (PGMs). It is the least dense in PGMs and has the lowest melting point. Its basic properties are listed in Table 2. Among all the properties of Pd, the most appealing one is its ability to absorb hydrogen. Palladium can absorb up to 900 times its own volume hydrogen at room temperatures; this property is quite specific to only hydrogen. It is this property that makes Pd the perfect media in hydrogen storage applications.

2.5.2 Hydrogen Palladium System

As mentioned above, Pd is selected as an important candidate in hydrogen related applications because of its unique properties towards hydrogen. First of all, upon introduction of hydrogen under room temperature, the chemical state of Pd changes [44]. As shown in Figure 2.5.1(A),

two different phases of palladium hydrides, including alpha (α) phase and beta (β) phase, exist when hydrogen is introduced. At room temperature or higher temperatures, α phase Pd hydride has a very low atomic ratio of H/Pd (<0.1), while β phase Pd hydride has a much higher atomic ratio (H/Pd≈0.7). These two phases can coexist when the atomic ratio is in middle range. Figure 2.5.1(B) shows that the composition of Pd changes accordingly with the hydrogen partial pressure. Under certain environmental pressure and temperature, the higher hydrogen concentration results in a higher hydrogen partial pressure. Thus, this figure indicates that the phase of Pd hydrides formed is directly dependent on the actual concentration of hydrogen. With lower hydrogen concentration (or partial pressure), the hydride would be α phase and β phase hydride forms with higher hydrogen concentration. The transition from α phase to β phase is reversible when the hydrogen concentration changes. Also, the relationship between the Pd hydride composition and hydrogen pressure under different temperature has been studied in detail [45] and used in sensor working temperature selection.

Table 2 Basic Properties of Palladium

Name/Symbol/Number	**Palladium/Pd/46**
Group/Period/Block	10,5,d
Appearance	Silvery white metallic
Standard Atomic Weight	106.42 $g \cdot mol^{-1}$
Phase	Solid
Density (room temperature)	12.023 $g \cdot cm^{-3}$
Crystal Structure	Cubic face centered
Melting Point	1828.05K
Boiling Point	3236K
Electrical Resistivity	105.4 nΩ·m(20°C)

In accordance with the transition of the Pd hydride from α phase to β phase, two detectable effects occur which form the basis of many hydrogen sensors. First of all, a resistance increase occurs when the hydride shifts from α phase to β phase, as Figure 2.5.2 illustrates [46]. R_0 represents the resistance of palladium when H/Pd is 0. R represents the actual resistance of Pd. It is clear that the resistance change could be as high as 1.8 times at room temperature (solid circles) when the Pd hydride transforms from α phase (H/Pd≈0) to β phase (H/Pd≈0.7).

Secondly, a structural lattice change would happen. Palladium has an fcc structure with a lattice parameter of 0.3890 nm (298K). Upon hydrogen absorption, the lattice undergoes an isotropic expansion while keeping its fcc structure. In α phase (298 K), the lattice parameter of PdH~ is 0.3894 nm, which reflects its small component ratio of H/Pd (~ 0.015). However, in β phase, which co-exists with α phase, the lattice parameter is 0.4025 nm where the component ratio H/Pd is much higher (~0.7) [14, 44]. The volume expansion from α phase to β phase is around 10.4% [14, 44, and 45]. This 10.4% volume expansion could be a dominant effect when it comes to a nanosized structure.

Upon phase transition of PdH from α phase to β phase, the resistance would go up while the lattice expands because of higher H/Pd ratio. These two effects form a basis of understanding the mechanism of hydrogen sensors in the following parts.

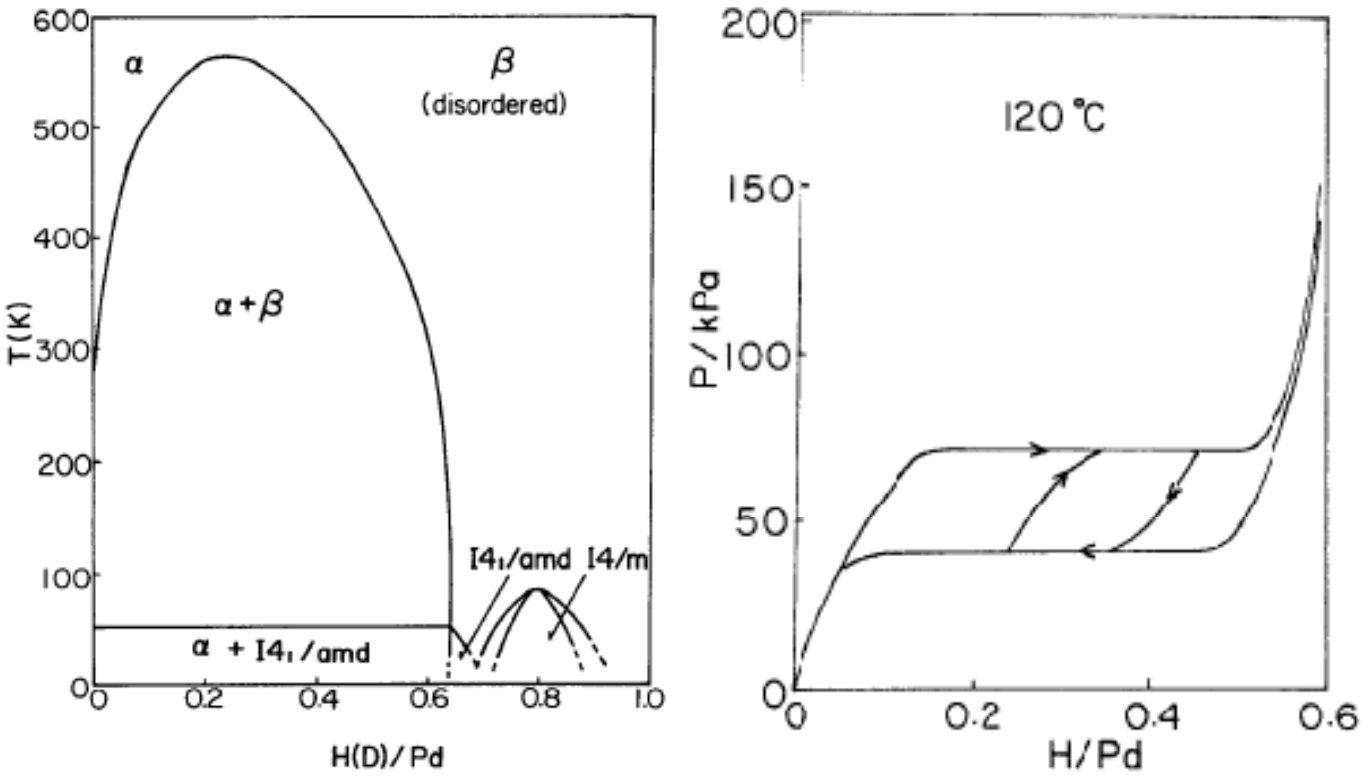

(A) (B)

Figure 2.5.1 (A) A phase diagram showing the existence of α phase and β phase Palladium Hydrides. (B) A hysteresis shown for Hydrogen Palladium system at 120°C [44]. Reprinted, with permission, from the Annual Review of Materials Science, Volume 21 (c)1991 by Annual Reviews www.annualreviews.org

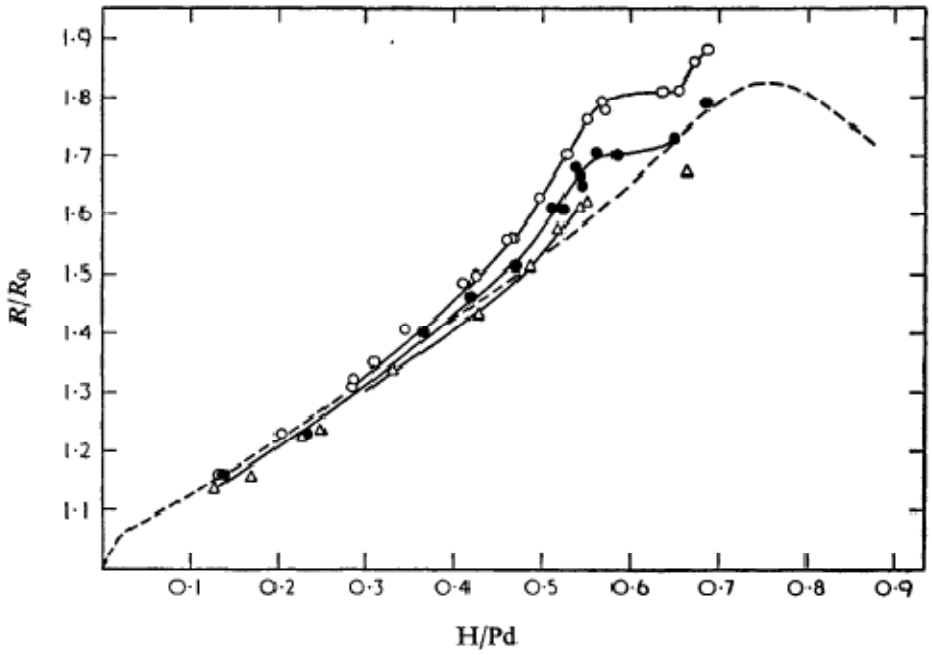

Figure 2.5.2 Relationships between H/Pd and R/R0. Hollow circle: 0°C; solid circle: 25°C; triangle: 50°C [46]- Reproduced by permission of The Royal Society of Chemistry.

.

3.0 EXPERIMENT

3.1 TEMPLATE PREPARATION AND NANOCHANNEL FORMATION

The key issue of our experiment is to discover how to fabricate thin and uniform Pd nanowires. In order to fabricate nanowires with diameters less than 100nm, we used electrophoresis to deposit Pd on a substrate with 100 nm wide channels which went across pre-patterned gold electrodes so that an electric field could be applied. This template was prepared using conventional microelectronic processes together with a lift-off step and an e-beam lithography step. Figure 3.1.1 illustrates the complete process.

We chose a (100) p type Si wafer as the substrate. In step A, a certain thickness SiO_2 is thermally grown working as an insulation layer. Two different thicknesses have been used: 100 nm and 150 nm. In steps B and C, the pattern of Au/Ti electrodes is transformed using optical lithography. In step D, a layer of 95nm thickness Au is deposited by e-beam evaporation. In order to increase the adhesion of the Au layer on SiO_2, a layer of 5nm Ti layer is deposited before deposition of Au. Then, the patterned photoresist is removed using warm acetone and Au/Ti electrodes are formed after lift-off. These electrodes will work as the conduction pads for both electrophoresis and wire bonding. Nanochannel is formed in steps E and F. In step E, a layer of 100 nm to 150 nm thick PMMA is spun on the substrate. After the e-beam lithography steps, nanochannels with 100nm diameters are formed in step F. A detailed recipe for e-beam lithography is shown in Table 2.5.1. The distance between electrode pads varies from 3 μm to 5

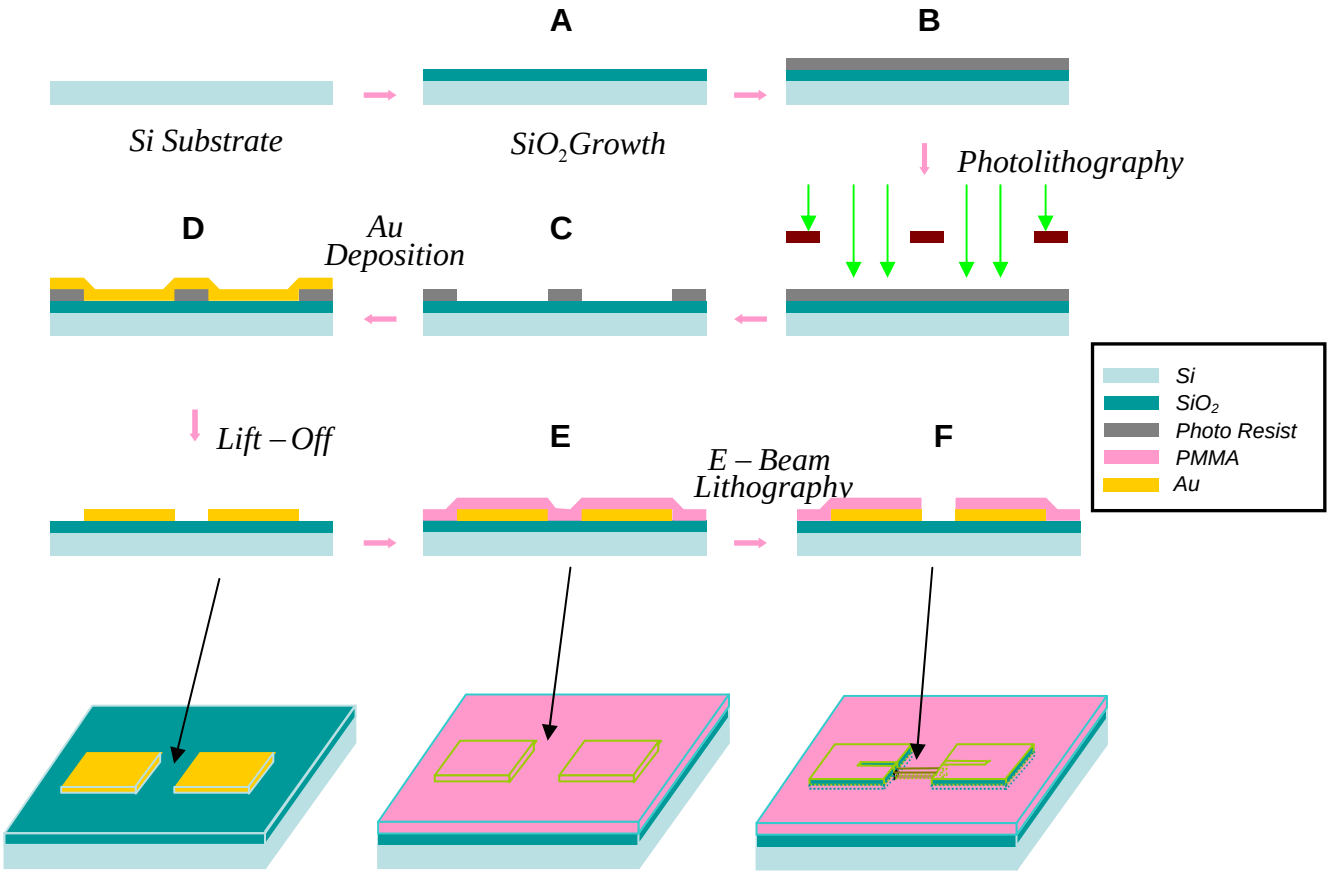

Figure 3.1.1 Fabrication process of template for 100 nm PMMA channels. A: 100 nm thick SiO2 growth; B: Photoresist spin-coating; C: Development of photoresist; D: E-beam evaporation of 5nm thick Ti layer as adhesion layer followed by 95nm thick gold layer as electrode. E: PMMA spin-coating; F: E-beam lithography and development of PMMA to pattern 100 nm wide nanochannels.

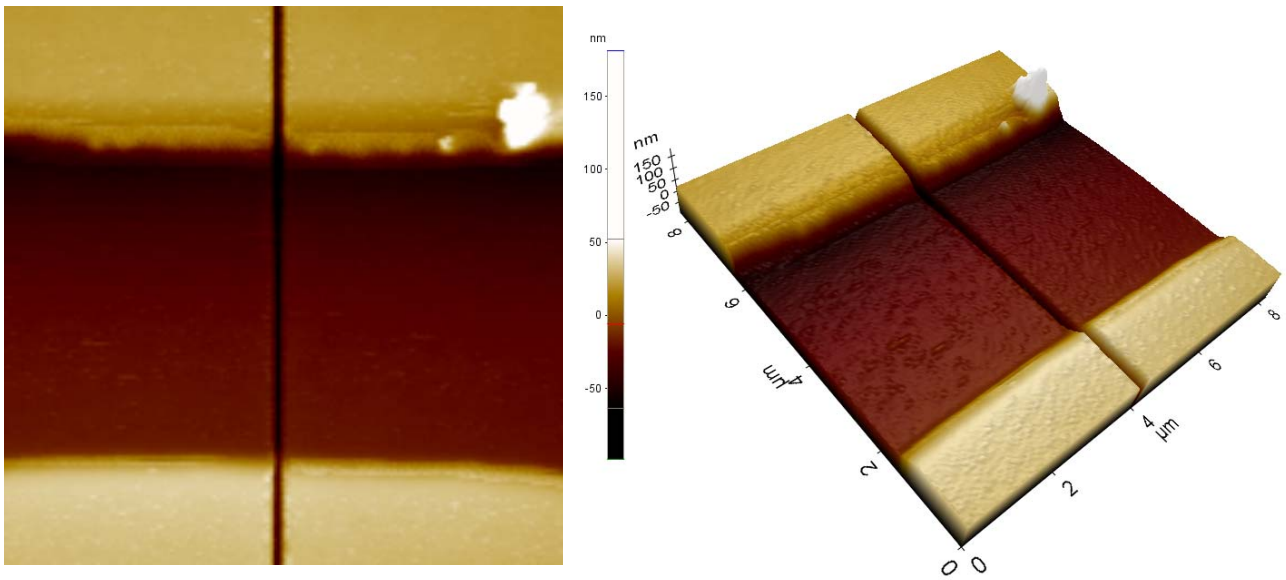

(A) (B)

Figure 3.1.2 (A) An AFM image of nanochannel together with electrodes on both sides. The size of the image is 8×8 μm^2 and the channel length is 4.5 µm. (B) The 3-D view of the channel and electrodes. The height of the electrode is 100 nm and the depth of the channel is 100 nm.

μm. These channels have a length of 20 μm going across the gap between the electrode pads. Finally, a channel with two ends connected to Au/Ti electrodes and the upper side opened to air is formed. Figures 3.1.2 A and B present AFM images showing the nanochannel between electrodes.

3.2 SINGLE NANOWIRE DEPOSITION VIA ELECTROPHORESIS DEPOSITION

Once the fabrication process of the template wafer is finished, the wafer is cut into small slices and ready for electrophoresis deposition.

3.2.1 Preparation of Electrolyte Solution

The process of Pd deposition is completed by placing a drop of solution on the nanochannel and applying an electric field through it. This electrolyte solution contains $Pd(NH_2)_2(NO_2)_2$ (Diamminepalladium Nitrite) and $NH_4SO_3NH_2$ (Ammonia Sulfamate) with concentrations of 10g/L and 100g/L, respectively [47]. In the solution, the two components would go through the following dissolution processes:

$$\mathrm{Pd(NH_2)_2(NO_2)_2} \leftrightarrow \mathrm{Pd^{2+} + (NH_2)_2(NO_2)_2^{2-}} \tag{3.1}$$

and

$$\mathrm{NH_4SO_3NH_2} \leftrightarrow \mathrm{NH_4^+ + NH_2SO_3^-} \tag{3.2}$$

Thus, this solution contains Pd^{2+} which works as the Pd source in electrodeposition. During the electrophoresis deposition process, the pH value of this solution is adjusted at around 7 by

adding H_3NSO_3 (sulfamic acid) and NaOH (sodium hydroxide) to avoid its reaction with Au electrodes or PMMA. The conductivity of the solution made ranges from 450 μS/cm to 600 μS/cm.

3.2.2 Nanowire Growth

The electrophoresis deposition of the Pd nanowire is finished in a probe station, as shown in Figure 3.2.1. The probe station consists of four separate probes with 1 μm diameter tips. Via coaxial cables, the probes are connected to a semiconductor analyzer (Agilent B1500A) which supplies electrical signals and collects data. In our experiment, we attach two probes to the electrodes on both sides of the channel. Then, we place a drop of Pd electrolyte solution (~0.5 μL) on the channel using a micropipette. After that, a constant current (10nA~500nA) is applied through the two probes; the voltage signals are collected and shown by semiconductor analyzer. Figure 3.2.2 (a) illustrates this process. By monitoring the voltage drop across the channel, we are able to tell whether the growth of the nanowire is completed. During the growth process, the Pd nanowire grows from one electrode (cathode) to another (anode), but the two electrodes are not connected. The expected voltage drop would be a few volts. Once the Pd nanowire connects the other electrode (anode) and the growth is completed, the resistance between the two electrodes drops dramatically; thus results in a sharp drop of the voltage signal, as shown in Figure 3.2.2 (b). The voltage in this case is around 100 μV to a few mV. The current should be stopped once the voltage drops to avoid further axial growth of the nanowire.

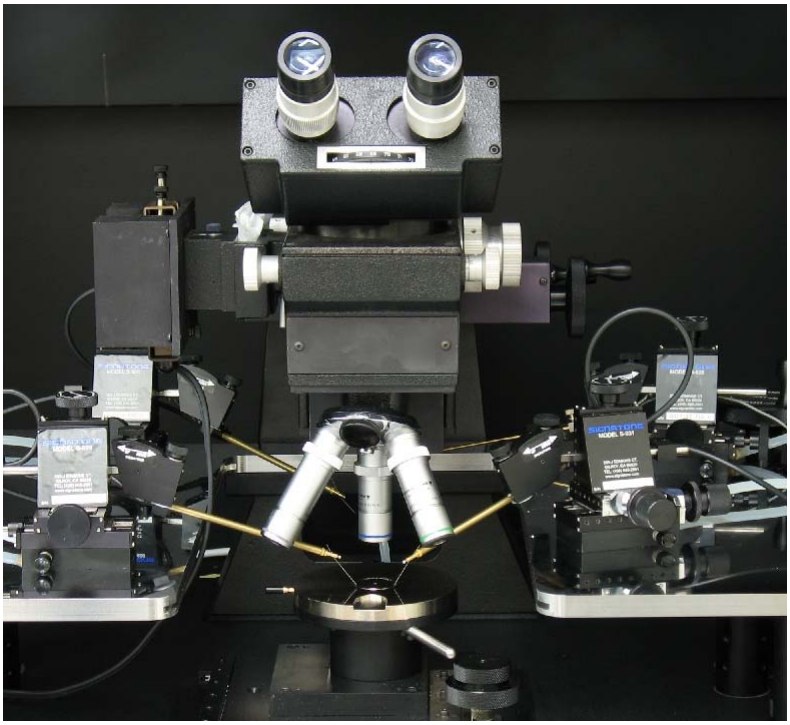

Figure 3.2.1 Probe station by The Micromanipulator Co. Inc.

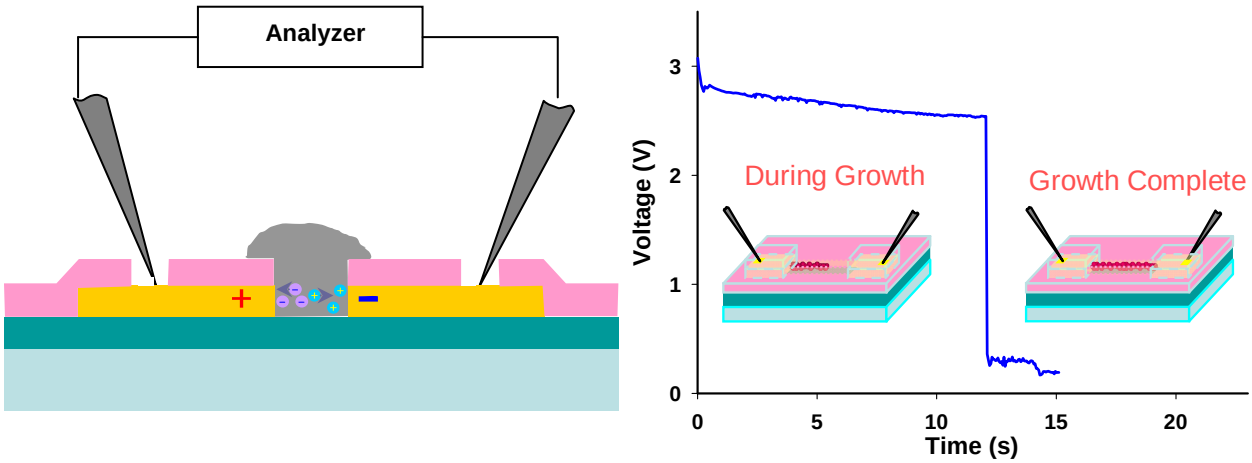

(A) (B)

Figure 3.2.2 (A) Two probes provide a constant current through the channel during growth. (B) Voltage drop appears when nanowire growth is completed.

3.3 INTEGRATION OF SENSOR DEVICES

In order to use the nanowires in hydrogen sensing, we have to integrate single nanowires into devices by adding external circuits. Wirebonding is the process of connecting the nanowire with an external circuit by bonding the electrode pads into outer pins on a slice holder.
The wirebonding process is finished on a manual wedge wirebonder provided by Kulicke & Soffa INC. The Au electrode pads are bonded by an Au wire with a 32 μm diameter through which it is connected to a pin of a slice holder. The slice holder is bought from Aegis Inc. An illustration of wirebonding and a finished device are shown in Figure 3.3.1 (a) and 3.3.1 (b), respectively.

3.4 GAS SENSING SYSTEM SET-UP

Once the nanowire is wirebonded to the slice holder, a sensor device is finished. In order to detect different concentrations of hydrogen, a gas sensing system, which is able to control the gas concentration and apply and detect the electrical signal, is required.

The gas sensing system used in our experiments is illustrated in Fig. 3.4.1. First of all, a Labview (National Instrument Inc., USA) program is built to control two gas lines, supplying hydrogen gas and nitrogen gas, respectively, via an MKS flow controller system (MKS Multi Gas Controller 647C, MKS Instruments Inc., USA). There are two different hydrogen gas sources. The first one is 10% hydrogen, and the second is manufacture certified 0.1% hydrogen with nitrogen gas as a balance gas (Matheson Tri Gas Inc., USA). To achieve the desired

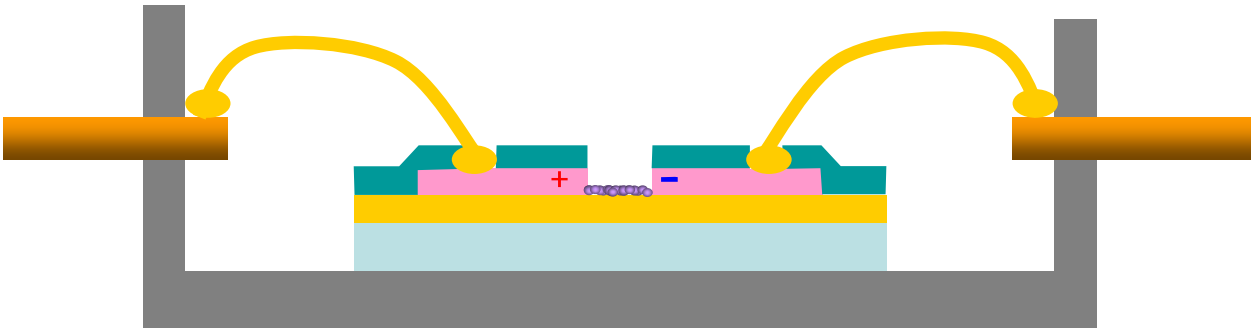

(A)

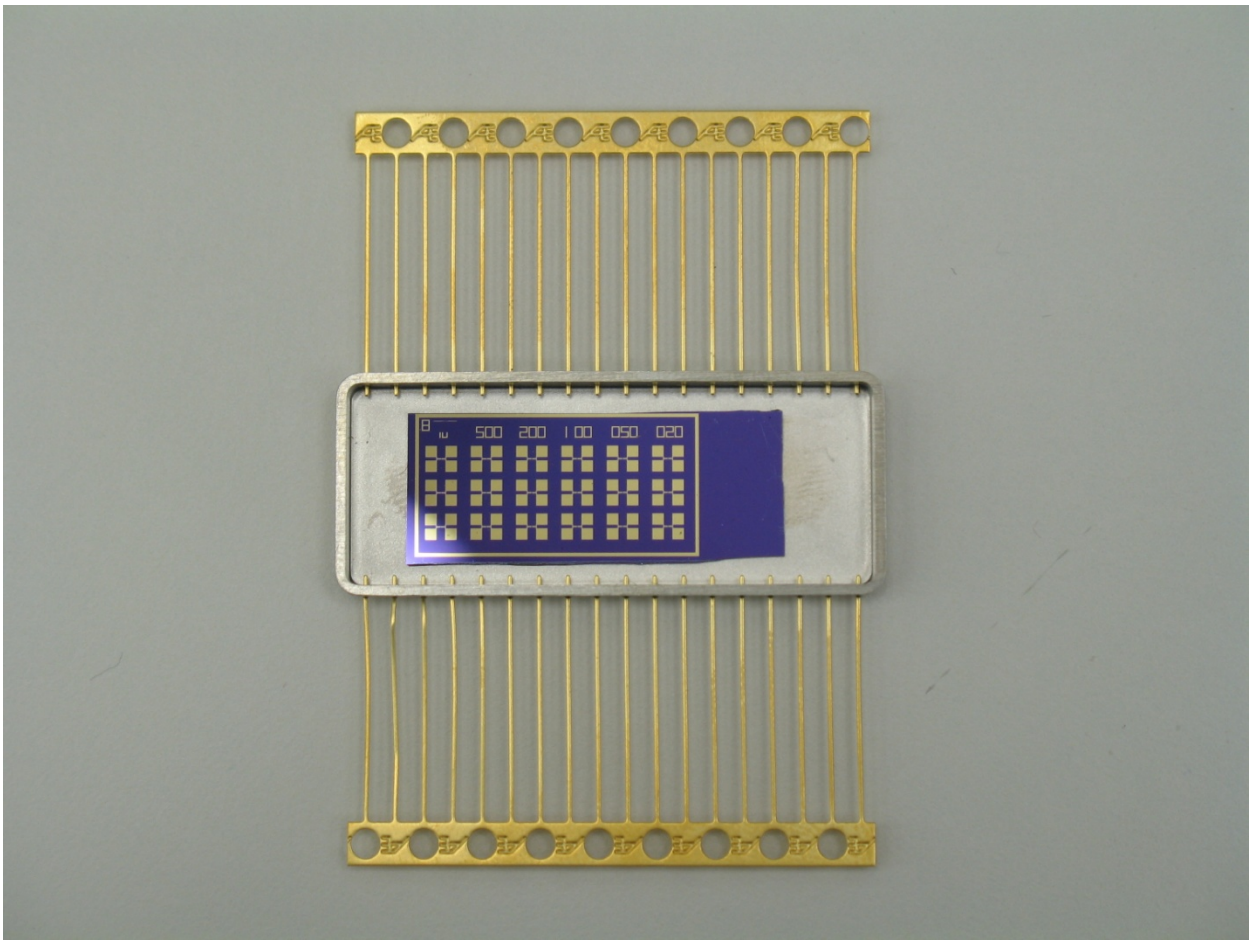

(B)

Figure 3.3.1 (A) Illustration of a sensing device with wirebonded nanowire. (B) A real image of sensing fabricated sensor device.

hydrogen test concentration, 99.999% pure nitrogen gas is used as a mixing gas to dilute the hydrogen. Two gas lines are connected to two MKS gas valves, as shown in Figure 3.4.2; the flow rates are controlled by the user through Labview system. The actual mixed gas concentration can be calculated by the following equation:

$$C_m = \frac{C_1F_1\times t + C_2F_2\times t}{F_1\times t + F_2\times t} = \frac{C_1F_1 + C_2F_2}{F_1 + F_2} \quad (3.3)$$

in which C_m, C_1, and C_2 represent the hydrogen concentration of mixed gas, gas 1, and gas 2, respectively. F_1 and F_2 represent the flow rate of gas 1 and gas 2, respectively. t represents time. Suppose gas 1 consists of 10% hydrogen, gas 2 is pure nitrogen, and C_1 and C_2 are 10% and 0, repectively. Because of the limitation of gas valves, F_1 can reach a minimum value of 1 sccm, while F_2 can reach a maximum value of 500 sccm. Therefore, C_m can reach any value from 10% to 0.02% (200 ppm) based on Eq. 3.3. If we replace gas 1 with 0.1% hydrogen gas, C_1 is 0.1%, C_m can reach any value from 0.1% (1000ppm) to 0.02% (2 ppm). With the proper flow rates of hydrogen gas and pure nitrogen, it is possible to produce any desired hydrogen concentration from 10% to 2ppm with this system.

To ensure proper gas mixing, the two gas lines are connected to a gas mixing chamber before going to the reaction chamber. The mixing chamber is a sealed small box with an inner volume of 12.6mL with two gas inlets connecting to gas lines and one gas outlet leading to the reaction chamber. The reaction chamber, where the nanowire sensor is placed, is a sealed plastic box with an inner size of 29.4 ml. There are two gas inlets, one of which is connected to a gas mixing chamber, while the other one is shut off. A gas outlet which directly connects to the ambient is on the back side of the chamber. The pins of the slice holder stretch outside the sides of the chamber and connect to the current amplifier, which is addressed in detail in part 3.5, via clip wires. Figure 3.4.2 shows the reaction chamber and the gas mixing chamber. In order to

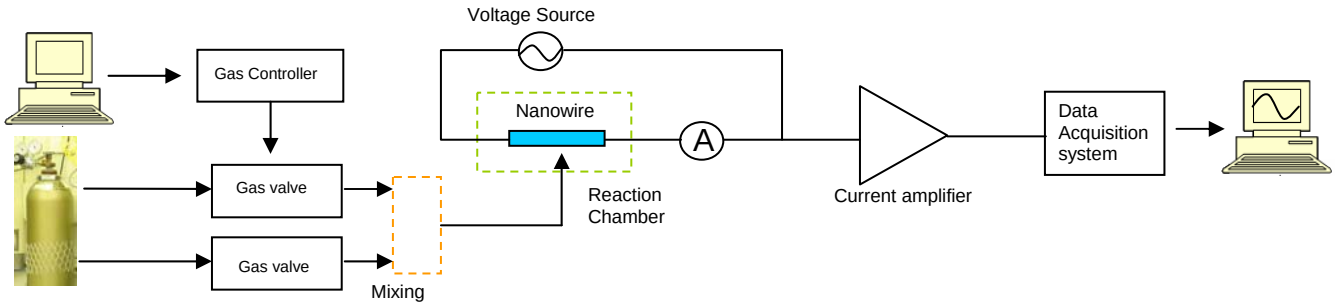

Figure 3.4.1 Sensing system set-up

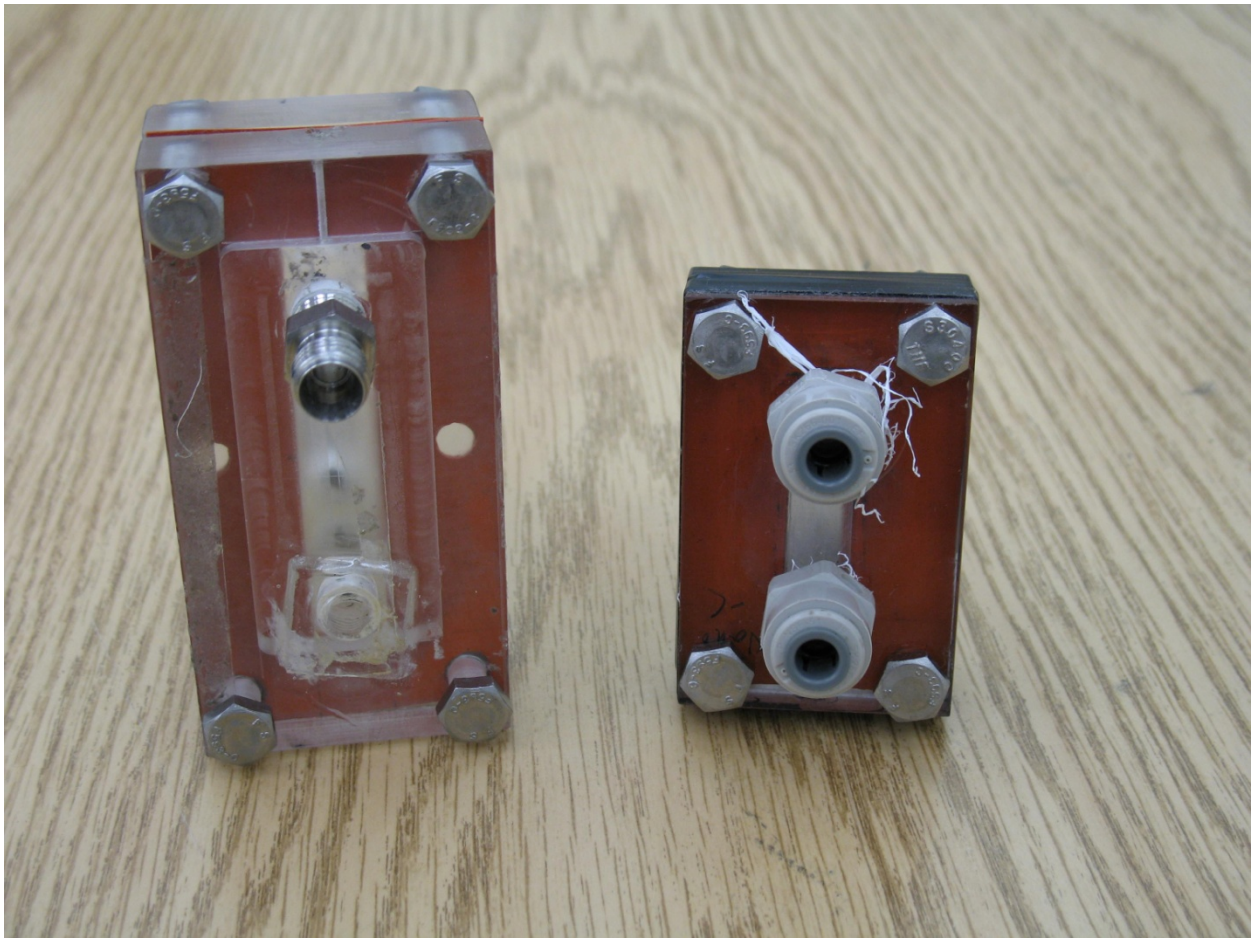

Figure 3.4.2 Reaction chamber (left) and gas mixing chamber (right).

reduce the effect of ambient noises, the sensing chamber is placed inside a metallic box which works as a Faraday cage. The sensing system does not require a pumping system and is operated at room temperature.

3.5 SIGNAL COLLECTION AND PROCESSING

In order to detect the resistance change of nanowires during hydrogen sensing, a constant DC voltage (~2.5 mV) is applied to the nanowire via a current amplifier (Keithley 428 Current Amplifier). This further collects the current signal running through the nanowire and converts it into a voltage signal proportional to the current signal. The output of the current amplifier is the converted voltage signal but with 10^3 to 10^7 amplification. This output signal is then connected with a data acquisition system (Keithley 2701) and recorded by Labview program. The final sensing chart based on collected data is plotted using a plotting software (Sigma Plot 9).

4.0 RESULTS AND DISCUSSION

4.1 NANOWIRE GROWTH AND PROPERTIES

By using electrophoresis deposition, we were able to successfully and constantly fabricated Pd single nanowires with diameters ranging from 50 nm to 100 nm. In order to study the surface, electrical, and structural properties of nanowires, we used a Semiconductor Analyzer, Optical and Scanning Electron Microscopy (SEM), and Atomic Force Microscopy (AFM) as characterization instruments.

After a nanowire is grown on the slice, it is cleaned by gently washing it in Deionized (DI) Water and then dried using pure dry nitrogen gas. An image of the channel and nanowire is taken using optical microscope (Carl Zeiss AG Reflected-Light Microscope) to verify the growth. An optical image with a magnification of 150×10 times is shown in Figure 4.1.1. As seen in the image, a channel formed by PMMA crosses both electrodes. PMMA is not clearly seen because it is very thin and clear. The nanowire is the dark tiny line inside the channel which can be barely seen. Since the maximum magnification is 1500 times, the diameter (~100 nm) is too small to be observed.

In order to further study the surface properties, an SEM system (Raith e-line) is used to take clearer images of the nanowires. The diameter of the nanowire ranges from less than 50 nm to over 100nm. A series of SEM images presented in Figure 4.1.2 show different nanowires with different diameters.

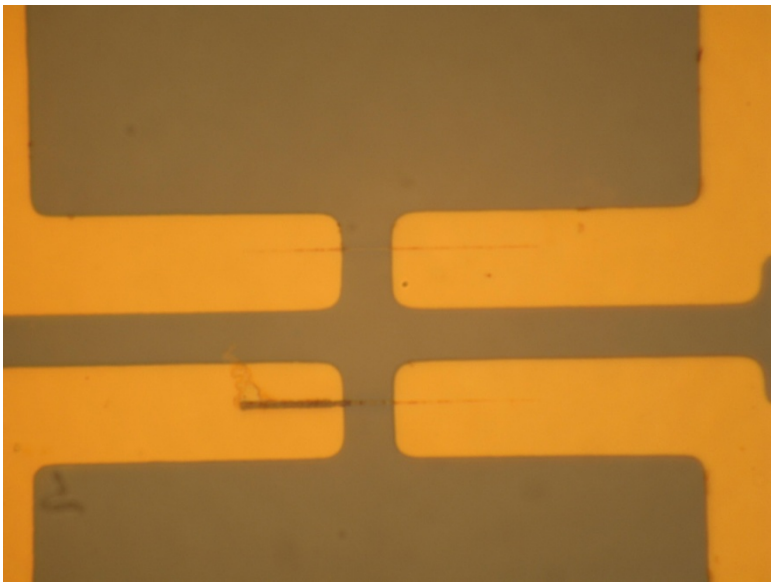

Figure 4.1.1 An optical image with 150×10 times magnification of a grown nanowire. There are two pairs of electrodes (yellow) and two channels (tiny lines between the electrodes). The nanowire grown, which is in the bottom channel, can be barely seen.

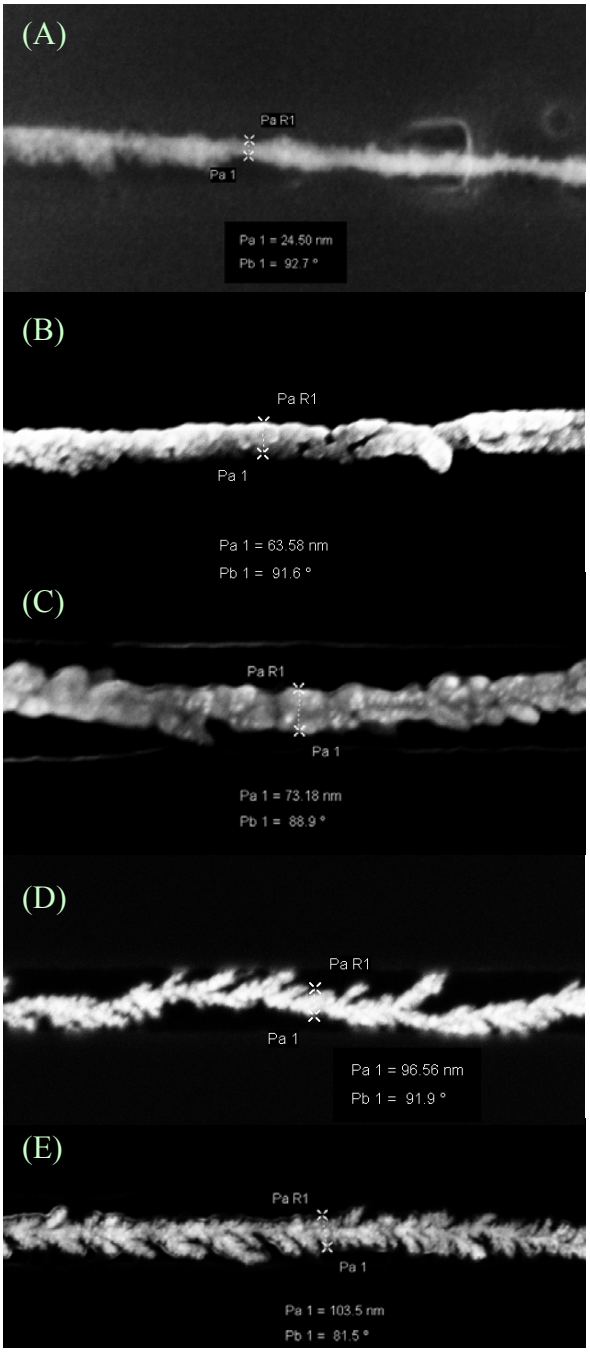

Figure 4.1.2 A series of SEM images for different nanowires with diameters of (A) less than 30 nm, (B) 63.58 nm, (C) 73.18 nm, (D) 96.58 nm and (E) 103.5 nm.

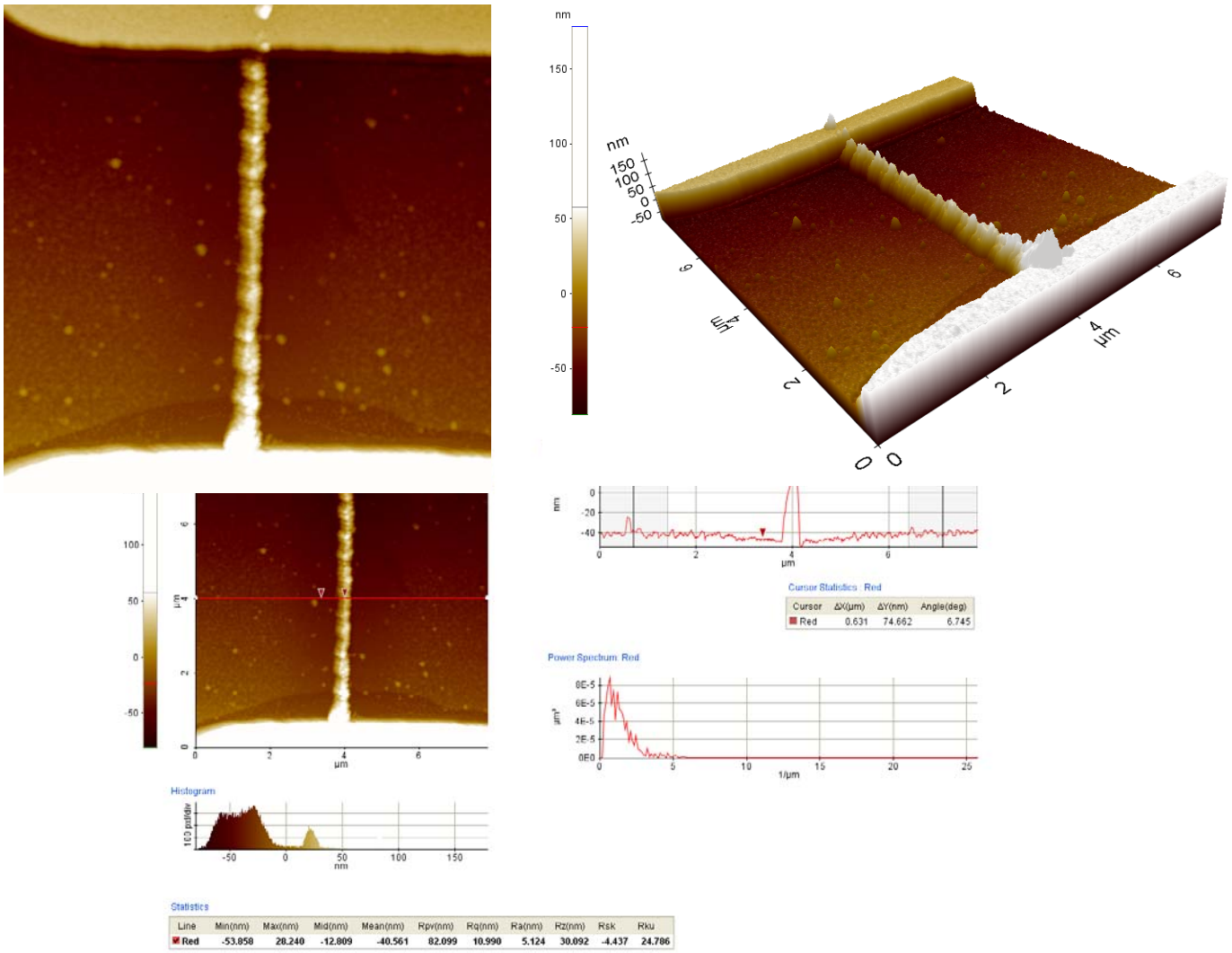

(C)

Figure 4.1.3 (A) An AFM image of a grown nanowire with 100 nm width and 6.5 µm length between electrodes. (B) A 3-D view of the nanowire and electrodes on both sides. (C) A line profile shows the height of the nanowire at around 74 nm.

AFM is used to detect the morphology of the nanowires. The nanowires are grown inside the PMMA channels with 100 nm thickness (as shown in Figures 3.1.2 A and B); thus, it is difficult to directly detect the nanowires using AFM because of the existence of PMMA. Because of this, we gently dipped our samples into warm (45°C) acetone for 5-10 minutes to remove the PMMA. After proper cleaning and drying, the nanowire is exposed on the surface and ready for AFM scan. In order not to damage the nanowire during scanning, a tapping mode is used. The AFM images of a grown nanowire are shown in Figure 4.1.3. Figures 4.1.3 A and B illustrate that the nanowire grown is very uniform in both width and height. The measured height of the nanowire from Figure 4.1.3 C is 74 nm, quite consistent with the 100 nm PMMA thickness.

The electrical resistance of the nanowire is tested using a semiconductor analyzer. As metallic material, the Pd nanowire shows a clear linear resistance over a range of voltage (from −3 mV to 3mV); resistances ranging from 100 Ω to over 10,000 Ω have been measured. The actual resistance of the nanowire primarily depends on three factors: physical dimensions, nanowire structures, and the connection between the nanowire and electrodes.

Physical dimensions refer to the diameter and length of the nanowire. Indicated by classical conductance law (Eq. 2.5), the nanowire's resistance is proportional to its length and inversely proportional to its cross-sectional area. However, our experiments showed only a weak connection not a clear trend that conforms to the law between resistance and length or diameter of nanowires. We attribute this to the fact that resistance also relies heavily on other factors.

The second factor is the actual structure of the nanowire. Nanowires grown are not ideal cylinders but have grain structures. They are neither really uniform in diameter nor in grain sizes. How the grains are grown and how well they connect with each other affects the actual resistance of the nanowires. The resistance of a nanowire is decided by its critical sites, such as the

narrowest part and the points where two grains connect to each other. This is the major reason why nanowire resistance does not conform to the classical law.

The connection between the nanowire and electrodes, especially the anode, is also critical. As the nanowire grows from cathode to anode, the growth process ends when the nanowire touches the anode. The connection could be very weak since the contact area between nanowire and electrode pad could be around, or even smaller than, grain size. Furthermore, there could be residual PMMA on both ends of the channel which stops the nanowire from fully connecting with the electrode pads. In order to have a good sensor performance, the nanowire must be kept in close and ohmic contact with the electrode pads so that the resistance change depends on the nanowire itself.

4.2 NANOWIRE STRUCTURES AND GROWTH CONTROL

As mentioned in part 4.1, a nanowire has different structures depending on the size of grains and how they connect together. In our experiments, we found three different kinds of nanowire structures: (1) plain structure, (2) grain structure, and (3) hairy structure. SEM images of these structures are shown in Figure 4.2.1 A to F. Plain structure nanowires, as shown in Figure 4.2.1 A and B, are composed of very tightly bound particles that are well connected to each other with no gaps. The diameter of this kind of nanowire is relatively uniform along the channel, and the surface is relatively plain. The grains in this structure are very well grown and connected. The grain structure nanowires, however, consist of small nano-sized grains, each barely connected to the others by a very small neck, as shown in Figures 4.2.1 C and D. The diameter of this kind of nanowire varies along the channel; the neck part can be as small as 10 nm or 20 nm. The typical

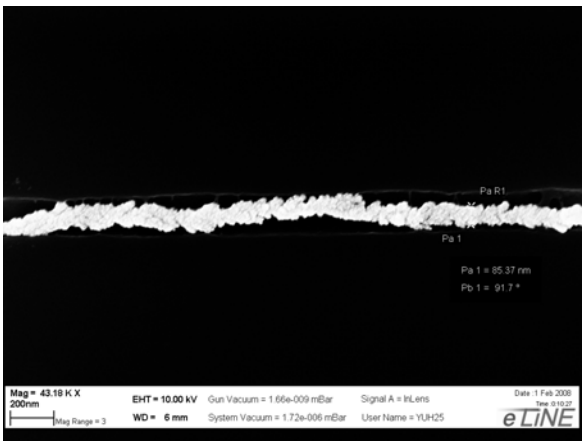

(A)

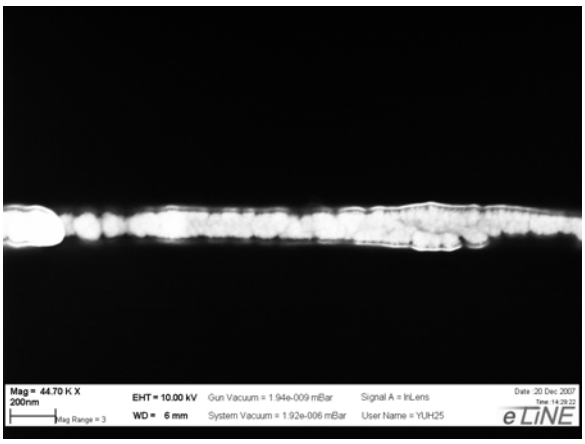

(B)

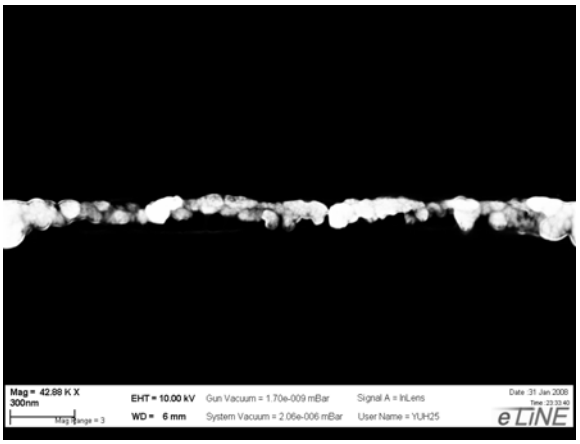

(C)

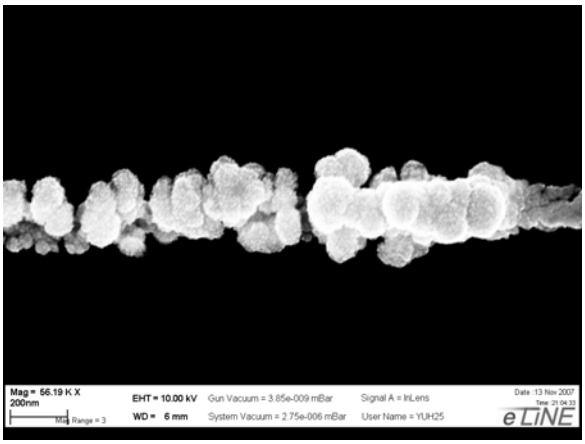

(D)

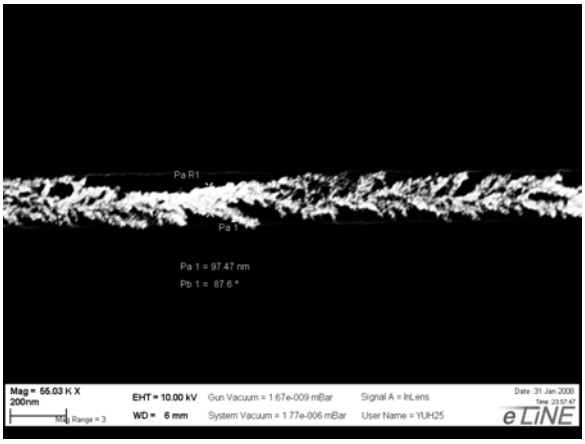

(E)

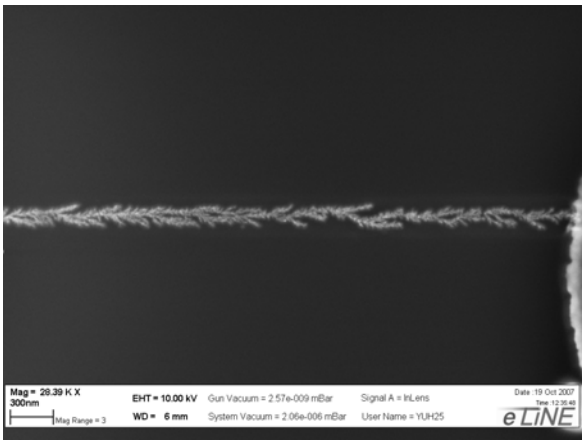

(F)

Figure 4.2.1. SEM images for three different nanowires structures: (A) and (B): Plain structure nanowires with 85 nm diameter; (C) and (D): Grain structure nanowires with diameter ranging from 100 nm to 150 nm; (E) and (F): Hairy structure nanowires with ~100 nm diameter.

size of individual grains or nodes ranges from 50 nm to100 nm. The grains in this structure are either not fully grown or too far apart from each other so that they barely connected each other. Hairy structure nanowires, shown in Figures 4.2.1 E and F, are similar to a tree structure. They have a trunk in the center and many dendrite-like branches reaching outward. The length of individual branches is limited by the width of the channel. In this structure, the grains are very small and the growth is very fast.

Through extensive experiments, we found that the structure of the nanowire is closely related to the electric field and current during growth. Based on this, we were able to control the actual structure of the nanowire. In these tests, the same 6 μm length and 100 nm width channels were used, while the growth current was varied. As shown in Figures 4.2.2 A to C, three SEM images with three different growth currents of 500 nA (A), 100 nA (B), and 50 nA (C) indicate a clear relationship between current and nanowire structure. With a higher current (Figure 4.2.2 A), the nanowire tends to grow fast, produce more dendrites, and form a hairy structure. With a lower current (Fig.4.2.2 C), the growth is comparatively slower and produces a grain structure. Interestingly, with an intermediate current, the nanowire could show grain structure on the cathode (left) side and hairy structure on the anode (right) side, as shown in Fig. 4.2.2 B.

A possible explanation could be reached by considering the deposition as a combined process of grain growth and electric field driven aggregation. During electro deposition, the grains already deposited are growing, while metal ions are driven by the electric field and attaching to the tip of grown nanowire, as shown in Figure 4.2.3. When a higher current is applied, the electric field in the channel is higher and the aggregation of metal ions is much faster than grain growth. Thus, the shape of the nanowire resembles that of diffusion limited aggregation [48] and the grains are notably smaller. While the current is smaller, a smaller

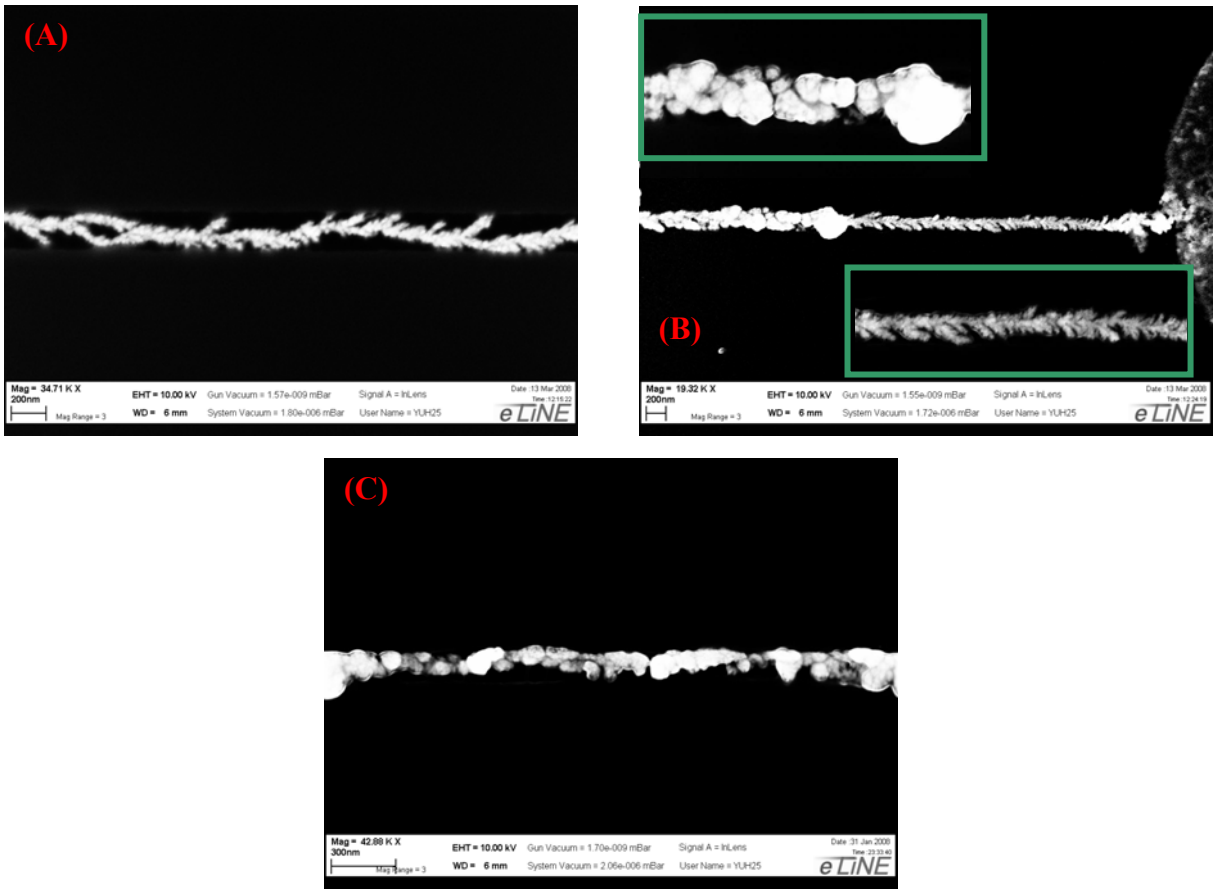

Figure 4.2.2 SEM images for nanowires grown using three different currents: (A) 500nA growth current; (B) 100nA growth current. The upper left inset is a magnification of the left side, and the bottom right inset is a right side magnification; and (C) 50nA growth current.

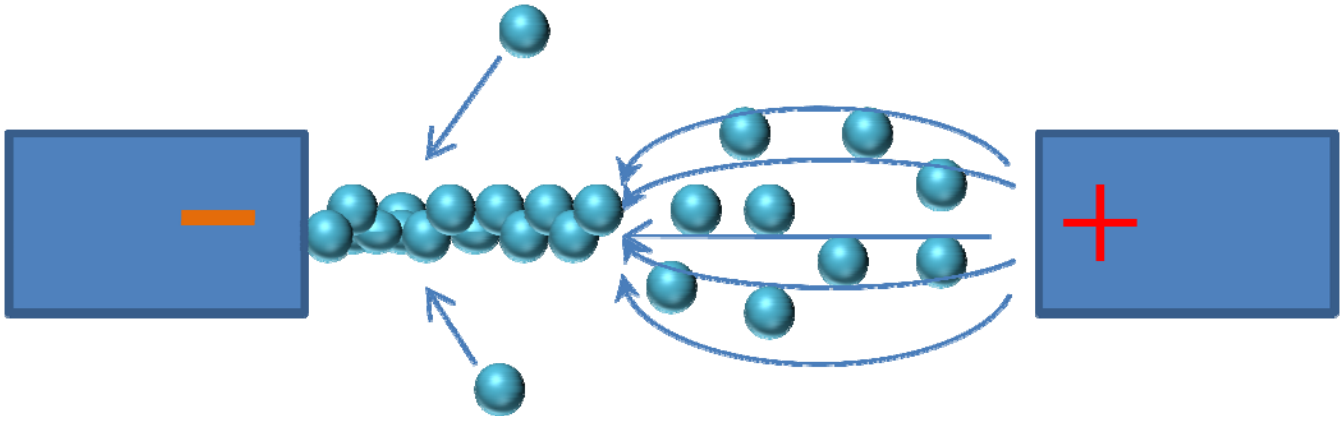

Figure 4.2.3 Illustration of nanowire growth process.

electric field is presented inside the channel. The grain growth is more favored as the nanowire grows slowly from cathode to anode. In this case, a nanowire with the grain structure is formed. With an intermediate current, the electric field inside the channel is small in the early stage of nanowire growth since the distance from the nanowire tip to the anode is large. Therefore grain growth is dominant in this stage when the nanowire grows from the cathode and the grain structure is forms in the cathode side. Since Pd itself is metallic and a good conductor, the electric field gets stronger and stronger between the nanowire tip and anode when the nanowire grows close to the anode**.** In this stage, growth speeds up and the hairy structure forms in the anode side. By setting a proper value of current using semiconductor analyzer, the structure of nanowires can be controlled.

4.3 HYDROGEN SENSING: PERFORMANCES AND MECHANISMS

The performance of a sensor can be characterized by the following factors: sensitivity, repeatability, and time. A great deal of hydrogen sensing of different hydrogen concentrations using fabricated naonwire sensors have been conducted and studied in detail.

(1) Sensitivity. The sensitivity of our devices is ultra high with a maximum value of 2-5 ppm. This value is the best sensitivity ever achieved using pure palladium and much better than similar hydrogen sensors made by Pd nanowire arrays [14] and Pd nanowire bundles [15].Figure 4.3.1 shows the sensing signal with 5ppm sensitivity. As indicated in the graph, when hydrogen is introduced into the sensing chamber, the voltage converted by the amplifier and collected by a data acquisition system showed a sharp increase. During the test, different hydrogen concentrations were introduced into the chamber, following a

1000 ppm – 100 ppm – 50 ppm – 20 ppm – 10 ppm – 5 ppm – 2 ppm – 1000 ppm – 100 ppm – 10 ppm – 5 ppm – 2 ppm manner. It is clear that the sensor is not only able to detect hydrogen with concentrations ranging from 10,000 ppm (1%) to 5 ppm (0.0005%) consistently, but it can also discriminate different concentrations with different signal heights.

(2) Repeatability. Repeatability, a key issue in sensor performance, characterizes the stability and reliability of a sensor. Our devices showed a very good repeatability during hydrogen detection, as shown in Figure 4.3.1 and Figure 4.3.2. In Figure 4.3.1, the sensing is repetitive, and the signal height is constant for the same hydrogen concentrations. In Figure 4.3.2, a sensing result with a same hydrogen concentration is presented. It is obvious that for the same hydrogen concentration (5000 ppm), the sensing is very repetitive with a fairly constant signal height. These results prove that the repeatability of our nanowire sensor devices is good. It should be noted, however, that the background signal of our devices has a certain drift. This drift could result from either hydrogen accumulation on the nanowire surface during sensing or the thermo effect of nanowire resistance. The drift undermines the reliability of devices and requires further research.

(3) Response time. Response time, which shows how quickly a sensor reacts to environmental change, can be characterized by rise time, which is defined as the time required for the sensor output to change from its initial state (10% value change) to a final value (90% value change). Fast response is critical in hydrogen detection, especially in aircrafts and spaceships where hydrogen leakage is quick and fatal. The single nanowire sensor devices in this work showed a good response time ranging from 9 seconds to a few tens of seconds. The real response time is even faster considering the

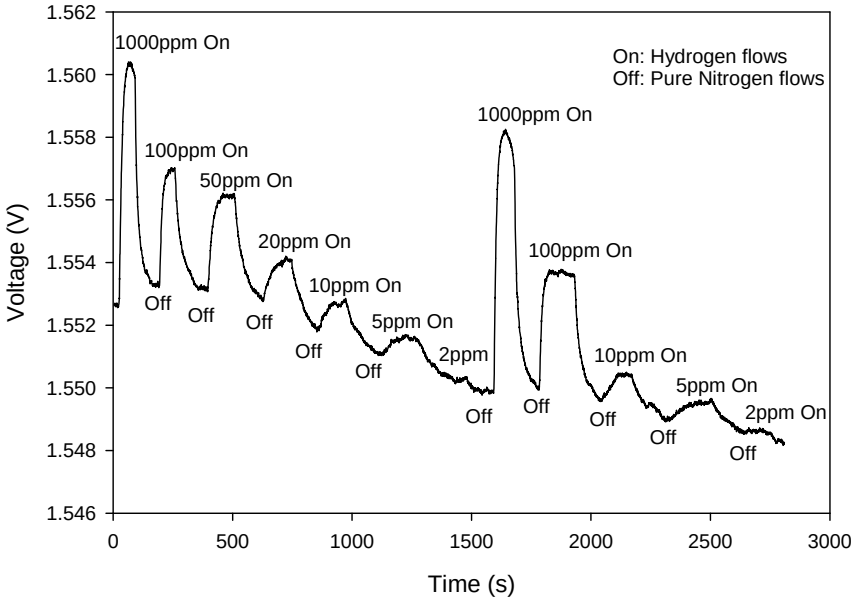

Figure 4.3.1. A sensing result of ultra high sensitivity with a 1000 ppm – 100 ppm – 50 ppm – 20 ppm – 10 ppm – 5 ppm – 2 ppm – 1000 ppm – 100 ppm – 10 ppm – 5 ppm – 2 ppm sensing order. It is a positive signal.

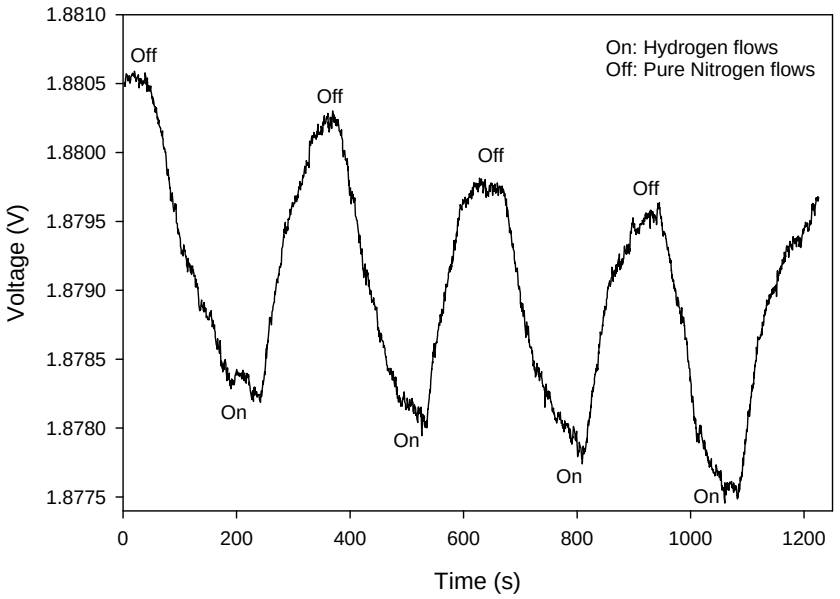

Figure 4.3.2. A sensing result of 5000 ppm hydrogen gas with negative signals.

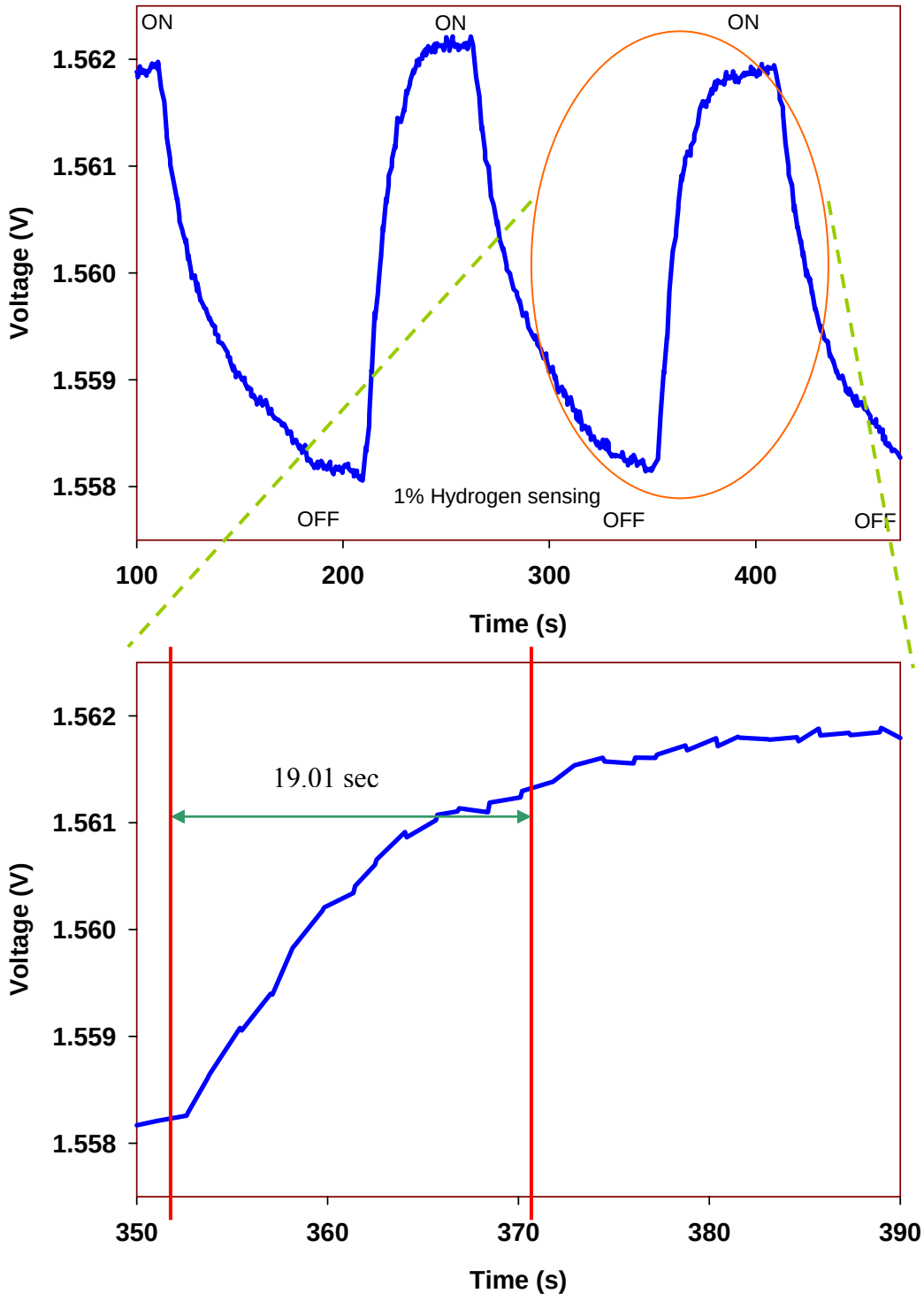

Figure 4.3.3. A sensing result of 1% hydrogen with positive signal. The rise time is around 19 seconds.

diffusion time from the tank to the sensing chamber. As shown in Figure 4.3.3, a 1% hydrogen sensing shows a response time of roughly 19.01 seconds and proves the fast response of single nanowire sensors.

In addition to the basic studies of hydrogen sensors, a new phenomenon was discovered during the tests. Rather than reacting to hydrogen in the same way, the different nanowire sensors showed diverse manners of resistance change upon the introduction of hydrogen. Taking a closer look at Figure 4.3.1 and Figure 4.3.2, the signal change directions of the two nanowires differ when hydrogen is presented. In the former graph, the voltage signal presents a sharp increase when hydrogen is introduced; this means a decrease of resistance happens. In the latter one, however, a sharp decrease of the voltage is presented, indicating an increase of nanowire resistance when hydrogen is presented. This phenomenon reveals that sensing mechanisms of Pd nanowires could be different, even if they are fabricated in the same way.

In order to fully address this issue, detailed research based on three different structures has been conducted. As mentioned in part 2.4.2, two effects could happen to Pd nanowires when exposed to hydrogen: resistivity increase and volume expansion. Because volume expansion often results in an increase of contact area between grains, a decrease of resistance occurs. For easier discussion, we call the voltage increase (or resistance decrease) during hydrogen exposure a positive signal, since the voltage goes up. The voltage decrease (or resistance increase) is called a negative signal since the voltage goes down. The two opposite effects work together with the final direction of resistance change depending on the dominant effect.

For the plain structure nanowires, measurements showed negative signals when exposed to hydrogen. The original resistance was recovered after nitrogen purged the sensing chamber. An SEM image of a plain structure nanowire is shown in Figure 4.3.4; its sensing signal of 5000

ppm hydrogen is shown in Figure 4.3.2. The diameter of the nanowire approximated 100 nm; the voltage drops (or nanowire resistance increases) when exposed to hydrogen. This can be explained by considering the two effects together. Upon a phase change from α phase to β phase, Pd (PdH_x) shows a resistivity increase of 1.8 times, which would result in 180% increase of resistance. The size expansion (3.36% lattice constant expansion), however, would result in a contact area increase of 6.8%, decreasing the resistance of the nanowire by 6.8% at the most, according to Eq. 2.5. It is obvious that resistivity change is dominant and the final trend is a resistance increase, thereby causing a negative signal to appear.

For the grain structure nanowires, positive signals were mostly seen in the sensing tests. Also, grain structure nanowires were found to have the highest sensitivity. The sensing signal in Figure 4.3.1 is a positive one; as shown in Figure 4.3.5, the nanowire used in this device has a grain structure. This nanowire has many tiny contact areas (necks) between two grains. The size of each neck is from less than 20 nm to 50 nm, and the grain size is from 50 nm to 100 nm. Because of its special structure, the volume expansion effect becomes more important than resistance change. Resistivity change still results in a 180% increase of resistance, while the volume expansion results in a more resistance decrease compared to the plain structure. In Figure 4.3.5, the green boxes are magnified images of grain structures in the nanowire. Consider a pair of grains together with a tiny neck between them. Two causes of size expansion of the neck area exist: 6.8% increase because of its own 3.36% lattice expansion; and a much bigger increase because of the compression from neighboring grains. Since the sizes of the grains are 50 nm to 100 nm and the size of the neck is typically 20 nm to 30 nm, the volume expansion of the neighboring grains has a strong impact on the neck. It forms an impressive stress which pushes the neck from both sides and greatly increases the contact area. An illustration of this mechanism

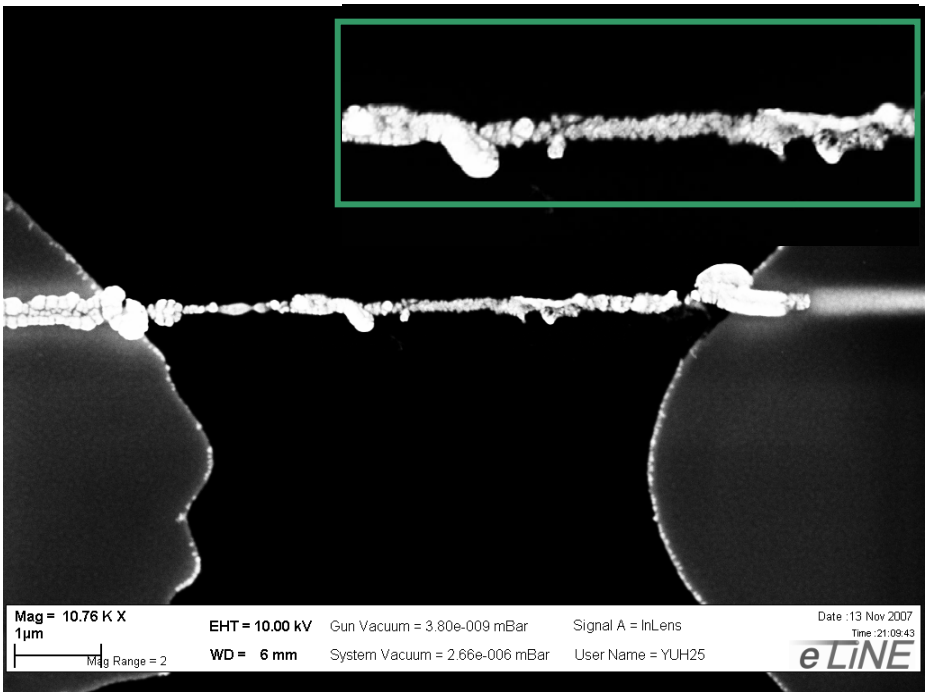

Figure 4.3.4 SEM image of a plain structure nanowire with a negative signal. This nanowire has a diameter of 100 nm and length of 6.5µm.

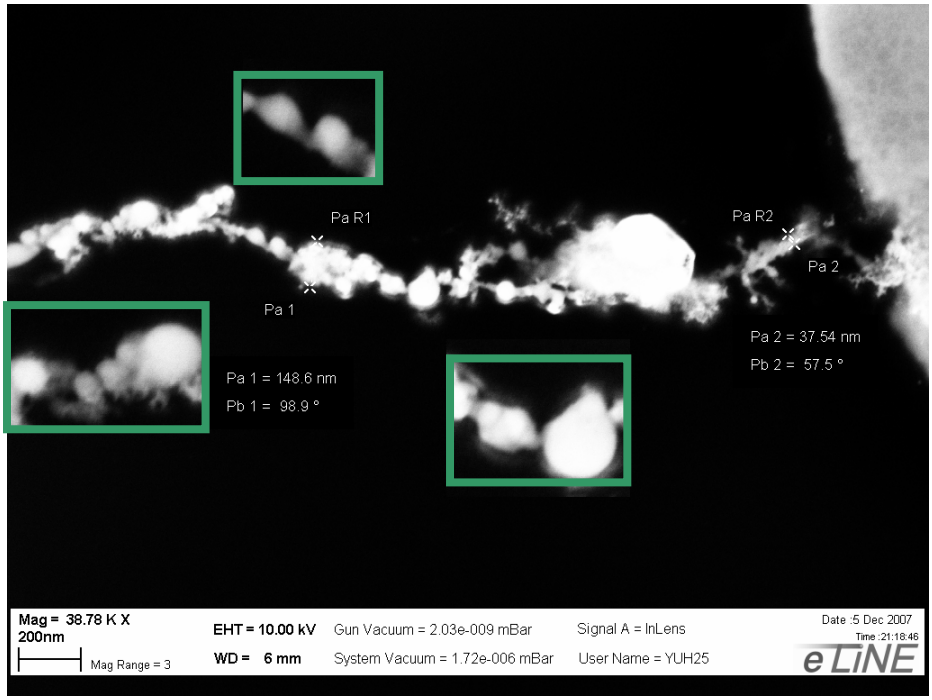

Figure 4.3.5 SEM image of a grain structure nanowire with a positive sensing signal. This nanowire has a diameter from around 150 nm to less than 30 nm; its sensitivity is 5 ppm.

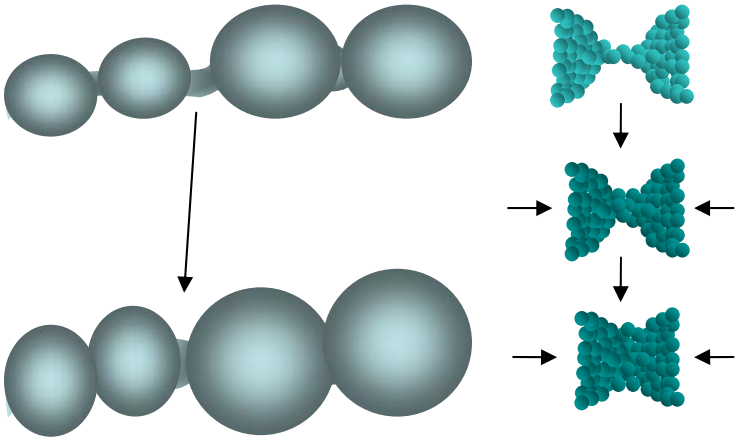

Figure 4.3.6. An illustration of the sensing mechanism of positive signals. The left side picture shows the change of neighboring grains and the size change on the neck. The right side picture shows the magnified view of the neck structure.

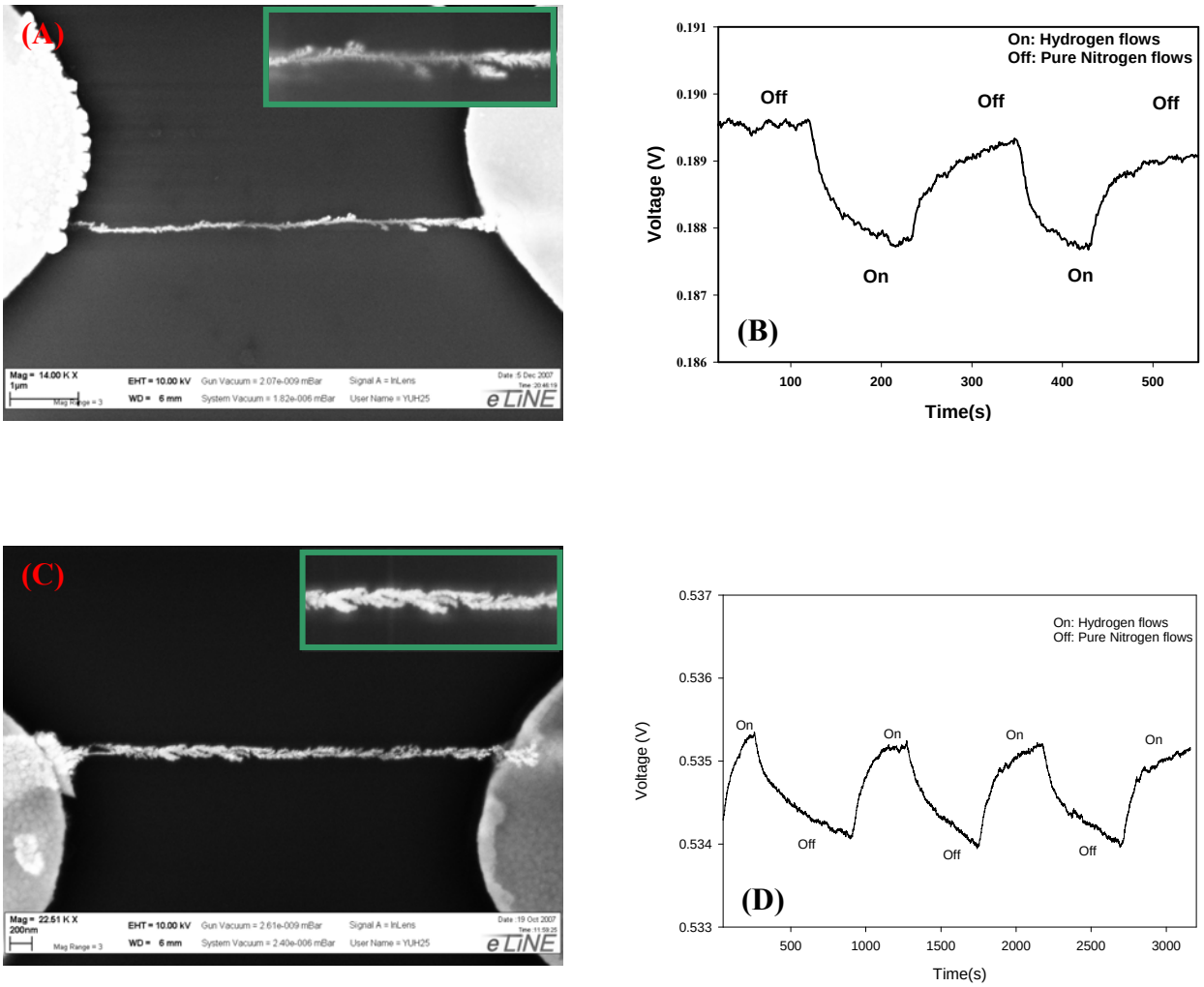

Figure 4.3.7. (A) SEM image of a hairy structure nanowire. (B) 1% sensing signal of nanowire A. (C) SEM image of another hairy structure nanowire. (D) 1% sensing signal of nanowire C.

is shown in Figure 4.3.6. Upon the introduction of hydrogen, the above two effects join together and result in a large increase of the contact area between neighboring grains, resulting in a big decrease of resistance. The area increase, which can be a few times larger than the 180% resistivity change, caused a positive signal to appear.

The hairy structure has a more complicated sensing mechanism than those of the plain structure and grain structure. Interestingly, above mentioned two different sensing signals both can happen in hairy structure nanowires. Figures 4.3.7 A to D present SEM images of two different hairy structure nanowires and their corresponding sensing signals. In Figures 4.3.7 A and C, two different hairy structure nanowires are shown. Their structures differ from each other. Nanowire A has a clear trunk with fewer dendrites which are far apart from each other, while nanowire C has no clear trunk but does have many dendrites which twist together with very small gaps. Figures 4.3.7 B and D illustrate their sensing signals. Nanowire A has a negative sensing signal, while nanowire C has a positive one. The presence of two different sensing mechanisms can be explained as follows: In nanowire A, the volume change of the nanowire does not add more contact area than plain structure nanowires since the dendrites are too far apart and the gaps between them cannot be closed with 10.4% size expansion. In this case, resistivity change is dominant, causing nanowire A act in a similar way to that of a plain structure nanowire. In nanowire C, however, far more dendrites exist with smaller gaps between them. Upon exposure to hydrogen, the size expansion of dendrites connects them and results in a larger contact area, similar to that of grain structure nanowires. Thus, a positive signal appears in this case.

Therefore, two different sensing signals have been found, and possible mechanisms have been proposed for the three different nanowire structures. More detailed research is needed, though, to fully address the structural and electrical change of the Pd nanowire upon exposure to hydrogen.

4.4 GATE ASSISTED NANOWIRE GROWTH

Pd single nanowires with a 100 nm diameter or less have been successfully and repeatedly fabricated using the electrophoresis deposition method described above. Their function as an effective and ultra sensitive hydrogen sensor has been approved by integrating them into sensing circuits. However, a more effective fabrication method, with a much higher success rate, a shorter growth time (higher throughput), and a better nanowire structure (more uniform, etc), is needed to further improve this process and demonstrate its promising future.

Rather than merely applying a one directional electric field to grow nanowire, we propose a new idea of adding another electric field to assist and control the growth. This other electric field is applied from an external electrode on the sample surface through the silicon substrate to the channel, forming a back-gate-like structure as shown in Figure 4.4.1. In order to fabricate the Au gate, we add an extra photolithography step before Au deposition. In this step opening areas were patterned and etched on SiO_2. These opening areas will be further deposited with gold which will work as gate. Three probes are used in this configuration: Probes A and B, like the previous configuration, connect to a DC current for nanowire growth. Probe C is the extra probe on which a constant DC gate voltage (V_g) is applied. The effect of the extra gate voltage on the nanowire growth inside the channel needs to be considered. Band diagrams and the distribution

of Pd ions inside the channel without a back-gate electric field (V_g=0), with positive gate voltage (V_g>0) and negative gate voltage (V_g<0) are shown in Figures 4.4.2 A, B and C, respectively. In these cases we assume that the silicon substrate is lightly p doped.

As shown in left side of Figure 4.4.2 A, a Schottky barrier $q(\varphi_m - \varphi_s)$ exists between the gold electrode and silicon substrate when no gate voltage (V_g=0) is applied. φ_m and φ_s represent the work function of gold (5.1 eV) and silicon (~4.52 eV), respectively. In this situation, a lightly accumulation of holes exists at the boundary between gold and silicon. No extra charge carriers exist in the channel or SiO_2 side, however, because the light accumulation of holes is recovered by the recombination in silicon. The right side of Figure 4.4.2 A shows the distribution of Pd^{2+} under this condition. Because of the existence of the lateral electric field applied from anode to cathode, the positive ions would move toward cathode, which results in a higher density of ions in the cathode side. In other parts of the channel far from the cathode the ions are relatively evenly positioned. This is the normal case when nanowire is grown using one directional electric field.

In the left side of Figure 4.4.2 B, a positive gate voltage (V_g) is applied on the gold electrode and results in an opposite bending of silicon conduction and valence bands. This could result in a depletion layer at the boundary of the silicon and gold electrode. Again, no extra charge carriers exist in the SiO_2 side. When V_g is big, however, there could be an inversion layer existing at the silicon and gold boundary with certain amount of extra electrons. This again would not affect the extra charge carriers in the SiO_2 side because of recombination. The resulted distribution of Pd^{2+} ions is shown in the right side of Figure 4.4.2 B. Compared with the situation of V_g=0, almost no change presents. Pd^{2+} ions still gather around cathode and distribute

evenly in other areas far from cathode. Thus, positive gate voltage imposes minimal effect on the growth of nanowire.

Figure 4.4.2 C shows a band diagram (left) and distribution of ions under a negative gate voltage. As shown in the band diagram, an extra bending of conduction and valence bands of silicon substrates is presented and accumulation of holes at the boundary of gold and silicon is very obvious. This further accumulation of holes could cause the penetration of electric field from gold into the bulk silicon. Once V_g is big enough, the bending of valence and conduction bands might be able to cause an inversion or even accumulation layer of electrons at the SiO_2 side. This gathering of electrons could further pose an electric field that goes into the channel side and affects the distribution of Pd^{2+} ions, as shown in the right side of Figure 4.4.2 C. This electric field formed by electrons at the SiO_2 works as a pulling force on positively charged Pd^{2+} ions and forces them distribute close to SiO_2, or the bottom of the PMMA channel. Once the growth starts, the Pd^{2+} ions that could be aligned by the gate voltage quickly connect with each other and nanowires are formed at the bottom of channel.

The application of negative voltage has three effects on the nanowire growth: (1) A shorted growth time, (2) A smaller diameter, and (3) A more uniform structure. As mentioned above, the negative voltage could pose a pulling force on Pd^{2+} ions and force them distribute along the bottom of the channel. This redistribution greatly reduced the distance between Pd^{2+} ions and the movement of ions during nanowire growth, which results in a shorter growth time. The diameter of nanowire could be reduced because the pulling down force tends to limit the growth of nanowire inside the channel and restrict its lateral growth. As shown in Figure 4.4.2, a much more uniform distribution of Pd^{2+} ions is presented inside the channel because of the application of negative gate voltage, which directly helps a uniform growth of nanowires.

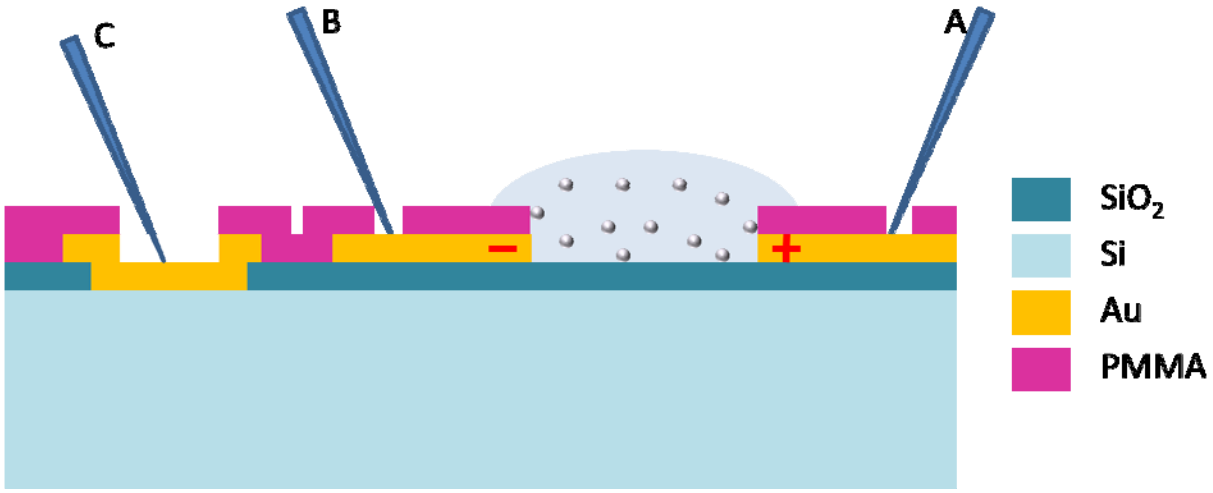

Figure 4.4.1 Illustration of gate-assisted nanowire growth set-up. A, B, and C represent three different probes that connect to the semiconductor analyzer. Probes A and B connect to growth current, while probe C connects to a constant DC voltage as a gate.

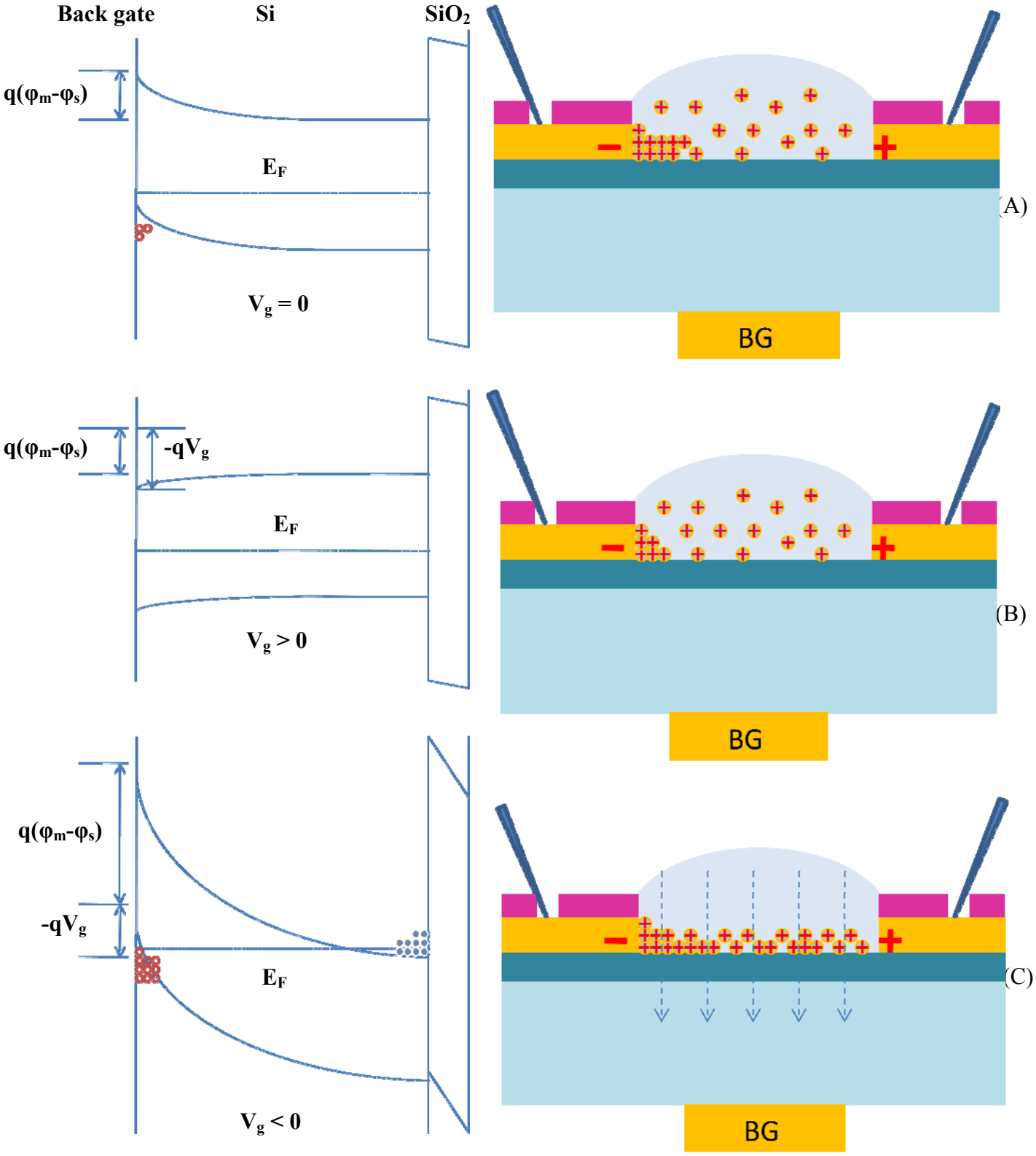

Figure 4.4.2 Band diagrams of the back gate structure (left) and illustrations of Pd^{2+} particles during growth (right) with (A) $V_g = 0$, (B) $V_g > 0$, and (C) $V_g < 0$.

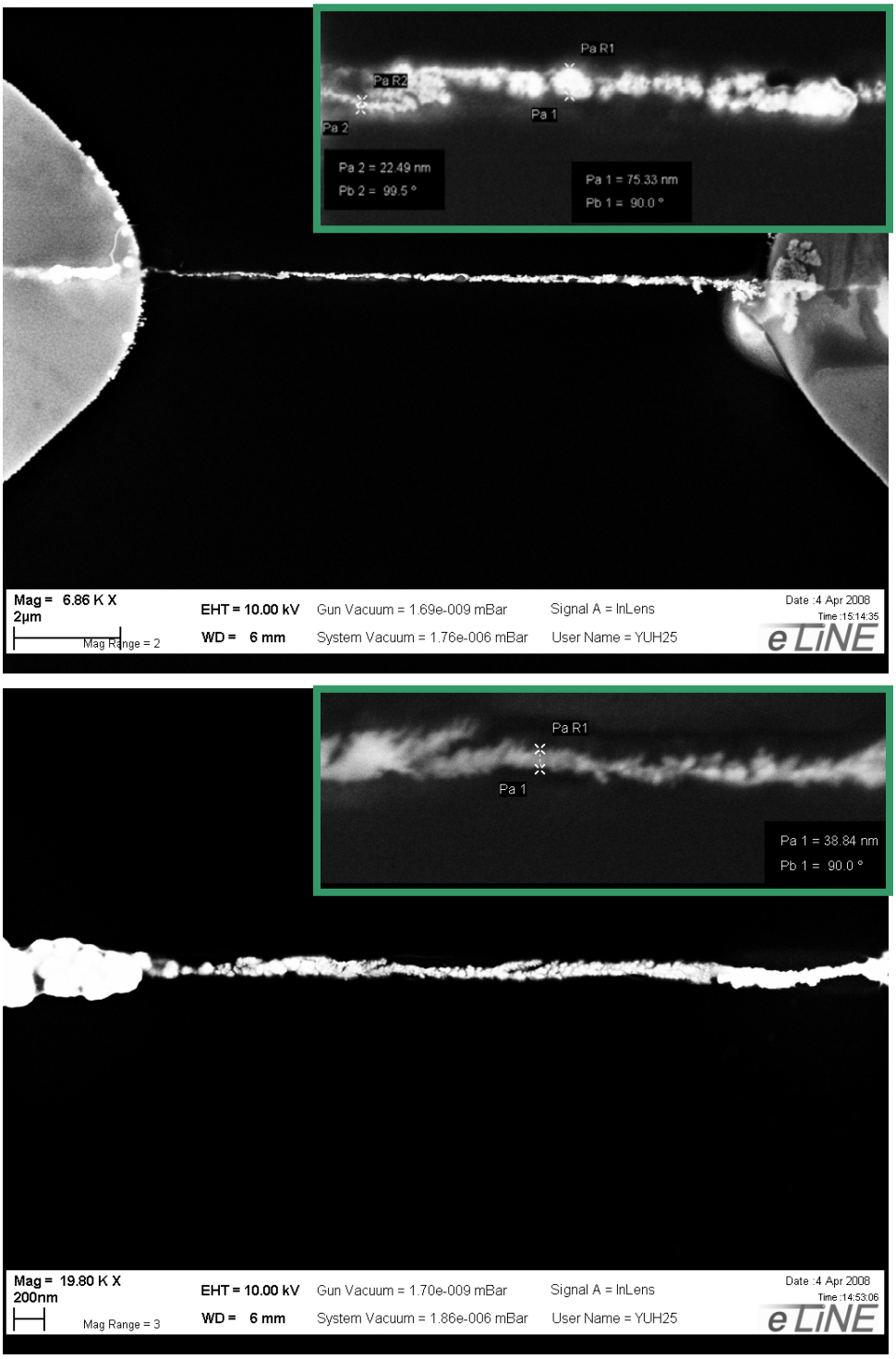

Figure 4.4.3 Two nanowires with small and uniform diameters. (A) A grain structure nanowire with its smallest part less than 23 nm, and (B) A hairy structure nanowire with its smallest part less than 38 nm.

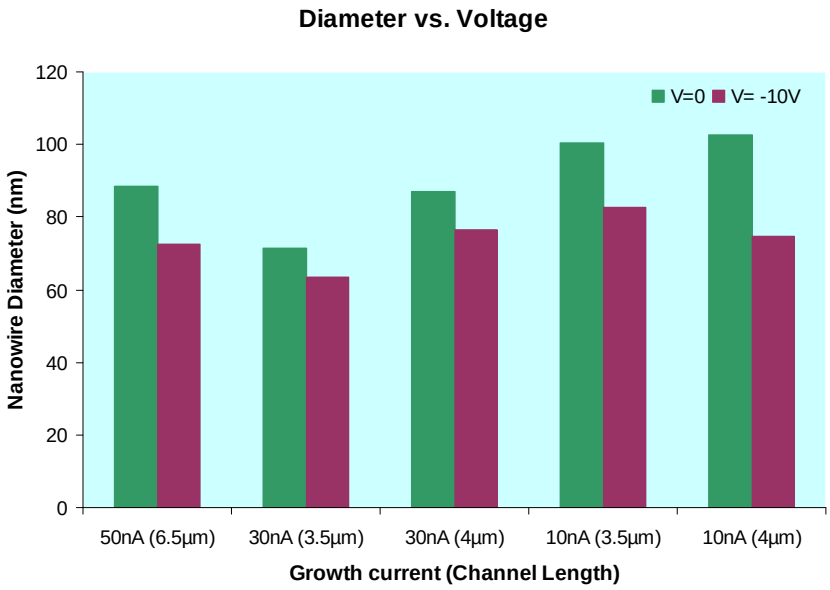

(A)

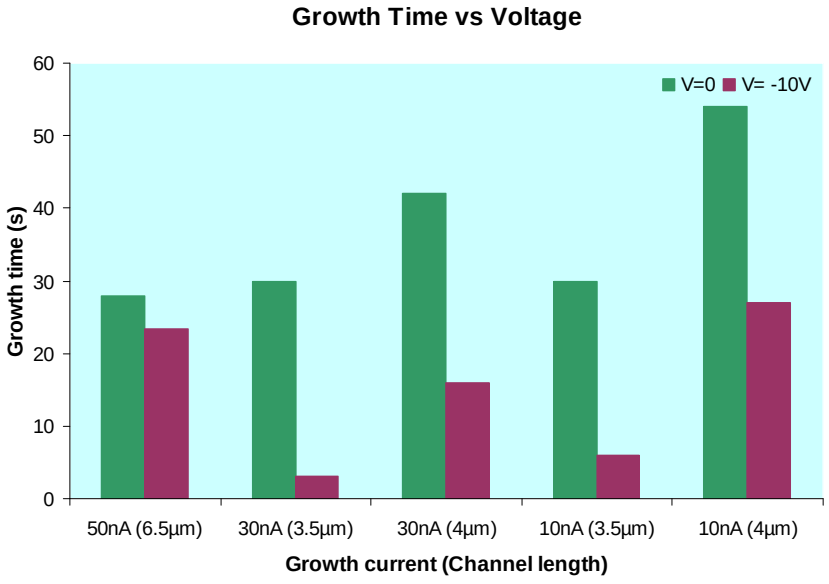

(B)

Figure 4.4.4 (A) The change of diameters from V_g= 0 to V_g= −10V under different conditions. (B) The change of growth time from V_g= 0 to V_g= −10 V under different growth conditions.

Experimental data prove the effects of the gate electric field. As shown in Figures 4.4.3 A and B, two nanowires with tiny diameters are fabricated using the gate-assisted growth method. Figure 4.4.3 is a grain structure nanowire, while Figure 4.4.3 B is a hairy structure nanowire. As shown in the images, the nanowires are quite uniform along a great distance, but the diameters are as small as 20 nm to 30 nm.

In order to further demonstrate the gate effect, a set of comparison experiments were done. Figures 4.4.4 A and B present the experimental data on diameter and growth time, respectively. Nanowires were grown under different growth conditions, such as growth current and nanochannel length with $V_g = 0$ or $V_g = -10V$. The growth currents had three different values: 50 nA, 30 nA, and 10 nA. There were three different kinds of channel length: 6.5μm, 4μm and 3.5μm length. Channel width remained the same at 100 nm in these three different kinds of channels. Figure 4.4.3 A shows that the nanowires grown with a gate electric field had smaller widths in all five different conditions. It is obvious that the usage of the gate electric field assisted the growth of the nanowire within the channels and shrinking the nanowire diameters. This idea can also be proved by the growth time change from $V_g = 0$ to $V_g = -10V$. Figure 4.4.3 B illustrates that the growth time with gate voltage is much smaller than that without gate voltage in five conditions - more than 50% in some cases. The decreased growth time results in a higher growth efficency and a higher throughput of nanowire fabrication. According to the relationship [14, 38]:

$$r(t) = \sqrt{\frac{2 I_{dep} t_{dep} V_m}{\pi n F L}} \tag{4.1}$$

where r(t) is the diameter of the nanowire, I_{dep} represents the growth current, t_{dep} represents the growth time, V_m is the molar volume of the deposited material, n is the number of electrons

transferred from the ion during deposition, and L is the total length of the channel. It is clear that diameter $r \propto t^{1/2}$. This relationship shows that the two charts are in accordance with each other.

Therefore, this gate-assisted nanowire growth is theoretically sound and, as proven in our preliminary experiments, this finding is very promising in controlling the nanowire growth and in obtaining thinner nanowire with higher fabrication efficiency. Furthermore, gate-assisted growth opens an entirely new idea of applying multiple electric fields from different directions during electrophoresis deposition.

5.0 CONCLUSION AND FUTURE WORK

5.1 CONCLUSION

In this work, we presented an effective way of fabricating palladium (Pd) metallic nanowires with less than a 100 nm diameter using electrophoresis deposition. PMMA nanochannels with 100nm width and 3.5 μm to 6.5 μm length were fabricated using e-beam lithography on the surface of a template. By applying a constant DC current through two gold electrodes, Pd single nanowires were electro-deposited inside these PMMA channel. AFM and SEM were used to characterize the surface properties of the single nanowires, while a semiconductor analyzer was used to test their resistance. SEM images showed that the nanowires grown were thin and straight, while AFM images showed that the nanochannels made by EBL were clean and uniform and the nanowires were vertically uniform with a height of around 100 nm.

Hydrogen sensors based on these Pd single nanowires were successfully integrated by wirebonding nanowires to wafer holders and then applying an external circuit, including a current amplifier, a data acquisition system, and a control system based on Labview. A gas sensing system based on a mass flow controller was set up; a hydrogen gas concentration from 10% to 2 ppm could be attained with proper control. The best tested hydrogen concentration yielded by our devices is 5 ppm, which is the optimum value we found in the literature for pure Pd hydrogen sensors. This result not only demonstrated the capability of Pd related

nanostructures in hydrogen detection, but more importantly, it also showed the advantage of a single nanowire structure in the sensor area.

Nanowire growth and sensing mechanisms were also studied in depth in this work. Three different nanowire structures were found, including plain, grain, and hairy structures. The growth mechanisms were discussed, and the growth control of nanowire structure was attempted by varying growth currents. In addition, two separate sensing signals were discovered when different nanowires were used in hydrogen detection. This phenomenon was not seen in other similar research. These experimental results suggest the need for a complete discussion on proposed different sensing mechanisms regarding three different nanowire structures.

This work also proposed and proved a novel idea of electrophoresis deposition. Rather than applying one direction electric field during growth, another extra electric field was applied inside the channel from the back gate by connecting the silicon substrate to a reverse biased voltage. This configuration helps pull down positive charged Pd^{2+} ions and the experimental results proved gate voltage's impact on nanowire diameter and growth time. Nanowires with tiny diameters and uniform structures were fabricated with a higher efficiency using this new gate-assisted growth. This idea opens a brand new vision of applying multiple electric fields during electrophoresis deposition that forms a 2D or even 3D electric field to achieve easier growth control.

5.2 LIST OF RESULTING PUBLICATION

[1] - Single Palladium Nanowire Via Electrophoresis Deposition Used as Ultra Sensitive Hydrogen Sensor, Yushi Hu (Department of Electrical and Computer Engineering, University of Pittsburgh, Pittsburgh, PA, USA), David Perello, Usman Mushtaq, and Minhee Yun. (Submitted)

5.3 FUTURE WORK

This work successfully demonstrated the growth of 50 nm to 100 nm diameter Pd single nanowires. Hydrogen sensors based on these nanowires were fabricated and used in detection; a fairy good sensitivity was achieved. However, this work mainly focused on the fabrication of metallic (Pd) nanowires and hydrogen detection. Also, with the diameter of nanowires approximately 100 nm, it was difficult to get down to less than 50 nm. Thus, developments of this project could go two possible ways: (1) other sensors based on different materials (biosensors based on conducting polymers), and (2) production of thinner nanowire.

Biosensor is becoming a more and more important device not only in biological and medical areas but also in environmental and social security areas [49]. Biosensor refers to a device that could detect a certain analyte and generate traceable electrical or optical signals. The applications of biosensors, such as detection of glucose for diabetes patients and detection of viruses in blood, have made them essential devices in hospitals and health related organizations. Biosensors are also becoming regular gadgets used by housewives to detect drug residual in foods or toxic substances in water. The remote detection of airborne bacterial makes them an

effective tool in the area of social security. In all, biosensor is emerging as a commonly used tool in a profitable market.

Biosensors based on nanowires have been proposed long ago by many research groups. Nanowire devices are suitable in this area because of their small size, high sensitivity, and low power consumption. Configured with the proper active elements on the surface of the nanowire, the existence of a certain analyte (i.e. glucose and DNA) would bind with the active elements and result in a change of the nanowire, such as conductance. This change is detectable and forms the basis of a sensor.

As a very promising candidate, conducting polymer, such as poly-pyrrole (PPy) and poly-aniline (PANI), has been extensively researched in integrating biosensors because of its special electrical and optical properties [50]. PPy and PANI nanowires fabricated using electrophoresis deposition have also been reported [51]. Given the reliability of a single nanowire growth method described in this work, single nanowire based on PPy and PANI can be synthesized with a small diameter as well as good surface properties by applying the gate-assisted growing mechanism.

An important advantage of nanowire based biosensors is their fast response and high sensitivity. As the change of signals is generated by the change of the properties of the nanowire itself, such as conductance, the one dimensional nanowire is easily affected by external change. The binding of an external charge could easily cause carrier depletion or accumulation in the nanowire; this process occurs quickly because of the nanowire's small diameter.

Another possible advantage of our nanowire sensor is the feasibility of Field Effect Transistor (FET) structure. As mentioned in part 4.4, a back-gate structure could be used to apply

another electric field to the channel. With a grown nanowire, the back gate forms an actual FET structure. Thus, a pre-aligned FET nanowire sensor device is easily obtained using our method; the sensitivity of this device could be optimized by tuning the gate voltage carefully.

The second route of developing this work involves thinner nanowires which can be made with the help of gate-assisted growth and the production of narrower PMMA channels. As proved in part 4.4, gate-assisted growth has a very obvious effect in limiting the diameter of nanowire; it simultaneously helps grow thinner and more uniform nanowires. On the other hand, PMMA channels can be made smaller to further restrict the growth of Pd nanowires during electrophoresis deposition. With a proper combination of EBL parameters and PMMA thickness, nanochannels with diameters less than 40 nm are obtainable [42]. In this case, the growth of nanowire could be further restricted by the channel; its diameter could be kept around 40 nm. The decrease of the nanowire diameter not only facilitates the study of the basic properties of nanowires, such as the relationship between nanowire diameters and the growth of thin nanowire using electrophoresis deposition, but it also elevates the sensitivity of nanowire sensors to another level because of the nanowire's reduced lateral size as well as increased surface to volume ratio.

APPENDIX

CONDUCTANCE OF SINGLE METALLIC NANOWIRE

As mentioned in part 2.2.1, the conductance of the nanowire can be expressed by Landauer's formula in (2.6). The T or transmission function in the formula is calculated using Green's functions of the central region and couplings to the leads [21]:

$$T = Tr(\Gamma_L g_c^r \Gamma_R g_c^a) \tag{A.1}$$

where Tr is the transmission coefficient, g_c^r and g_c^a are the retarded (r) and advanced (a) Green's functions of the center (c), and $\Gamma_{L,R}$ are functions for couplings to the leads (left and right). The central region, which is the computationally important part, may include tube junctions, defects, or vacancies. Therefore, any change in the atomic structure or the radius can induce changes among C, L, and R locations and alter the level spacing and the occupancy probability of the states. This, in turn, leads to detectable changes in conductance.

Electrical conduction in nanowires can be approximated as a ballistic scattering of electrons along the one-dimensional quasi-periodic super lattice of finite length [25]. Under this condition, the conductance of a specific nanowire should be decided by the number of states occupied by electrons existing in the nanowire while each electron state would contribute a conductance of G, which is expressed by Landuaer's equation in (2.6). Assuming that the

quantum states of the electrons in a nanowire correspond to the eigenstates of Schrödinger Equation:

$$-\frac{\hbar^2}{2m}\nabla^2\Psi(x,y,z) = E\Psi(x,y,z) \tag{A.2}$$

then we should be able to express the transmission coefficient as:

$$T = \sum_{n=0}^{\infty} T_n \tag{A.3}$$

where T represents the total transmission coefficient, n represents a specific quantum state number and T_n represents the transmission coefficient of the state n. By combining equation (2.6) and equation (A.3), we can find out the expression for nanowire conductance as [25]:

$$G = (2e^2/h)\sum_{n=0}^{\infty} T_n \tag{A.4}$$

Given a certain Fermi energy level E_F, since only the energy states E_n that are below E_F can be occupied by electrons while the states above E_F are empty, the states that contribute to conductance would be those below E_F. Based on this idea, the transmission coefficient of a certain state n can be expressed as:

$$T_n \approx \begin{cases} 0, & E_n > E_F \\ 1, & E_n < E_F \end{cases} \tag{A.5}$$

In this equation, we assume that the transmission coefficient equals 1 since in all cases it is very close to 1 [25]. By combining (A.4) and (A.5), we can express the conductance of nanowire as:

$$G = (2e^2/h)\sum_{n=0}^{N} T_n \approx (N+1)(2e^2/h), \qquad E_N = E_F \tag{A.6}$$

It is clear from (A.6) that the nanowire conductance is directly related to the total number of states (N+1) that is lower than the Fermi level. In other words, the conductance is decided by how many energy states are occupied by electrons.

As indicated by the above concept, conductance of the nanowire would decrease when the diameter of nanowire decreases, since fewer atoms in the cross section indicates less electron states that can contribute to the conductance. It is also predicted that as the diameter approaches the atom size, the conductance will change step by step instead of continuously. Multiple researchers have found these phenomena, and Figure A.1 illustrates a typical quantum conductance phenomenon in a global histogram from Ag nanowires [26].

In order to discuss how the conductance of nanowire changes with the diameter in detail, we can assume that the Fermi Level E_F in the nanowire stays constant as the diameter changes. We can then focus on how the energy of eigenstates changes using the Schrödinger Equation (A.2). It is obvious that we need to set a proper boundary condition to work out the energy of eigenstates. If we assume that the electron can only exist inside the nanowire structure and that the nanowire is a perfect cylinder structure with radius a and length L (as illustrated in Figure A.2), we can build the following equations [27]:

$$\begin{cases} -\frac{\hbar^2}{2m}\nabla^2\Psi(x,y,z) = E\Psi(x,y,z) \\ \Psi(x^2+y^2 \geq a^2, z \geq L) = 0 \end{cases} \tag{A.7}$$

If we assume that the nanowire structure is perfect in the z direction, given that the length of the nanowire is much larger than the radius (L>>a), we can transfer this problem into a cylindrical box. Note: Here we ignored the periodic atomic fields existing in the nanowire but assumed the space inside the nanowire to be a free space in order to simplify the situation and get a rough idea on how the energy states change with the diameter. In this case, the eigen energies to the

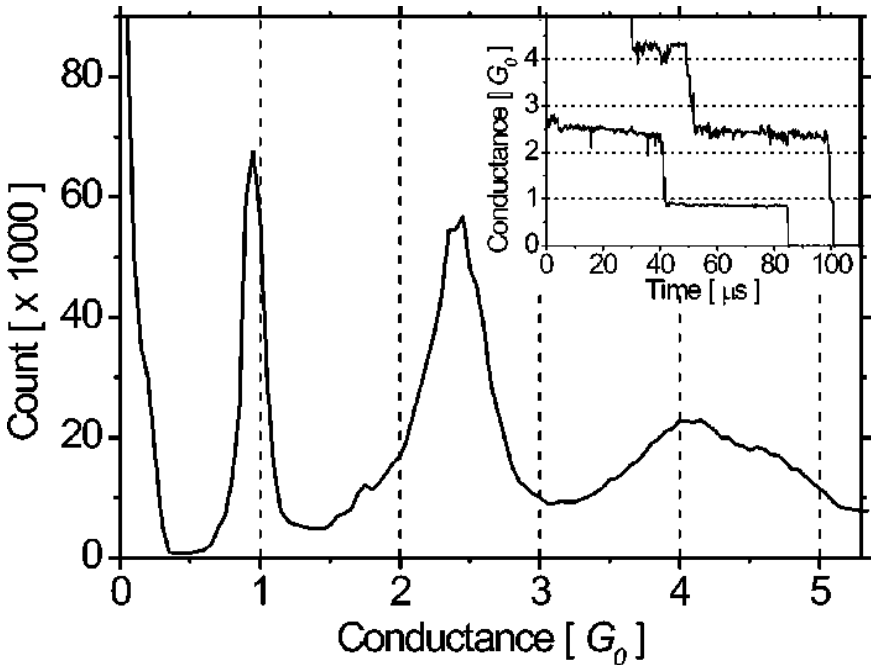

Figure A.1 Quantum conductance found in silver nanowires. Reprinted with permission from [26]. Copyright (2008) by the American Physical Society.

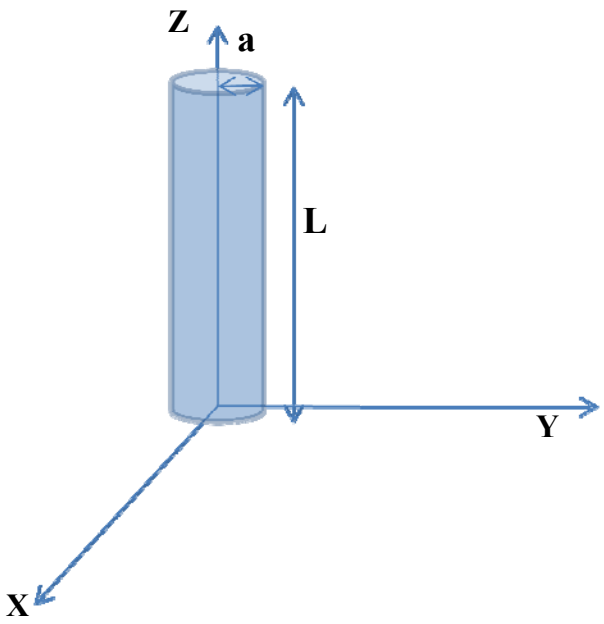

Figure A.2 Illustration of an ideal nanowire structure

cylindrical box could be expressed as [27]:

$$E_{nln_z} = (2e^2/h)[x_{nl}^2/a^2 + (n_z\pi/L)^2] , \quad J_n(x_{nl}) = 0, \tag{A.8}$$

where n, l, n_z are the eigen numbers in x, y, z directions, a is the radius of the nanowire, and L is the length. $J_n(x)$ is the Bessel function, and x_{nl} corresponds to the values that make this function zero. A few first zeros of the Bessel functions are listed in Table 1 [27]:

Let's consider the eigen energies given by (A.8). In the nanowire, it is assumed that L>>a. Therefore the second term on the right side of the equation can be ignored and (2.14) becomes:

$$E_{nln_z} = (\hbar^2/2m)(x_{nl}^2/a^2), \qquad J_n(x_{nl}) = 0 \tag{A.9}$$

For a specific eigen state, such as n=1 and l=2, the value of x_{nl} is set. A direct relationship between eigen energy E_{nlnz} and radius a can be found as:

$$E_{nln_z} \propto 1/a^2 \tag{A.10}$$

It is clear from (A.10) that as the radius of the nanowire is decreased, the energy of a certain eigenstate E_{abc} will be increased. From (A.6) the conductance of the nanowire is decided by the total number of eigenstates below E_F, and the number N means the Nth state which has the maximum energy under the Fermi Level. If radius a is decreased, E_N will be increased and lifted above the Fermi Level; no electron can occupy this state any more. As a result, the total number of the states below Fermi Level is decreased, thereby decreasing the conductance. Consequently, the decrease of conductance of the nanowire is directly related to the radius of the nanowire.

The conductance of nanowires is no longer decided by a classical relationship (2.5) because of the quantum transportation of electrons. A discussion between the conductance and nanowire radius based on Landauer's Formalism and ideal assumptions shows that the conductance is directly related to the radius and that the conductance decreases when the radius decreases.

Table 3 First few x_{nl} values to make Bessel function zero

	$l=1$	$l=2$	$l=3$
x_{0l}	2.40	5.52	8.65
x_{1l}	3.83	7.02	10.17
x_{2l}	5.14	8.42	11.62
x_{3l}	6.30	9.76	13.02

BIBLIOGRAPHY

[1]. Noboru Yamazoe, *Toward innovations of gas sensor technology*, Sensors and Actuators B 108 (2005) 2–14.

[2]. X. Bevenot, A. Trouillet, C. Veillas, H. Gagnaire, and M. Clement, *Hydrogen leak detection using an optical fibre sensor for aerospace applications*, Sensors and Actuators B 67 (2000) 57–67.

[3]. Hiroyasu Iwaharaa, Yamato Asakurab, Koji Katahirac, and Masahiro Tanaka, *Prospect of hydrogen technology using proton-conducting ceramics*, Solid State Ionics 168 (2004) 299–310

[4]. Magdalena Momirlana, and T.N.Veziroglub, *The properties of hydrogen as fuel tomorrowin sustainable energy system for a cleaner planet*, International Journal of Hydrogen Energy 30 (2005) 795 – 802

[5]. Constantinos Christofides and Andreas Mandelis, *Solid-state sensors for trace hydrogen gas detection*, J. Apply. Phys. 68 (6), 1990 R1.

[6]. Wei Lu and Charles M. Lieber, *Nanoelectronics from the bottom up*, Nature Materials 6 (2007) 841-850

[7]. Wei Lu and Charles M. Lieber, *Semiconductor Nanowires*, J. Phys. D: Appl. Phys. 39 (2006) R387-R406

[8]. Jiming Bao, Mariano A. Zimmler, Federico Capasso, Xiaowei Wang and Z. F. Ren, *Broadband ZnO Single-Nanowire Light-Emitting Diode*, Nano Lett., Vol. 6, No. 8, (2006) 1719-1722

[9]. Adam K. Wanekaya, Wilfred Chen, Nosang V. Myung, and Ashok Mulchandani, *Nanowire-Based Electrochemical Biosensors*, Electroanalysis 18, 2006, No. 6, 533 – 550

[10]. Zhiyong Fan and Jia G. Lua, *Gate-refreshable nanowire chemical sensors*, Appl. Phys. Lett. 86, 123510 (2005)

[11]. M. E. Bourg, W. E. van der Veer, A. G. Gruell, and R. M. Penner, *Electrodeposited Submicron Thermocouples with Microsecond Response Times*, Nano Lett., Vol. 7, No. 10, (2007) 3208-3213

[12]. Siegmar Roth and David Carroll, *One-Dimensional Metals*, WILEY-VCH Publishing, Weinheim, Germany, 2004

[13]. Fernando Patolsky and Charles M. Lieber, *Nanowire nanosensors*, Materialstoday, Apr. (2005) 20-27

[14]. Frederic Favier, Erich C. Walter, Michael P. Zach, Thorsten Benter, and Reginald M. Penner, *Hydrogen Sensors and Switches from Electrodeposited Palladium Mesowire Arrays*, Science Vol. 293 21 (2001) 2227-2231

[15]. Kyun Tae Kim, Sang Jun Sim, and Sung Min Cho, *Hydrogen Gas Sensor Using Pd Nanowires Electro-Deposited Into Anodized Alumina Template*, IEEE Sensors Journal, Vol. 6, No. 3, (2006) 509-513

[16]. Pai-Chun Chang, Zhiyong Fan, Dawei Wang, Wei-Yu Tseng, Wen-An Chiou, Juan Hong, and Jia G. Lu, *ZnO Nanowires Synthesized by Vapor Trapping CVD Method*, Chem. Mater. 2004, 16, 5133-5137

[17]. Minhee Yun, Nosang V. Myung, Richard P. Vasquez, Choonsup Lee, Erik Menke, and Reginald M. Penner, *Electrochemically Grown Wires for Individually Addressable Sensor Arrays*, Nano Lett., Vol. 4, No. 3, (2004) 419-422

[18]. S. Kagoshima, H. Nagasawa and T. Sambongi, *One-Dimensional Conductors*, Shokabo Publishing Co., Ltd., Tokyo 1982, Springer-Verlag Berlin Heidelberg New York

[19]. Andrew B. Greytak, Lincoln J. Lauhon, Mark S. Gudiksen, and Charles M. Lieber, *Growth and transport properties of complementary germanium nanowire field-effect transistors*, Appl. Phys. Lett., Vol. 84, No. 21, (2004) 4176-4178

[20]. Gregory S Snider and R Stanley Williams, *Nano/CMOS architectures using a field-programmable nanowire interconnect*, Nanotechnology 18 (2007) 035204

[21]. S. Ciraci, ABuldum, and Inder P Batra, *Quantum effects in electrical and thermal transport through nanowire*, J. Phys.: Condens. Matter 13 (2001) R537-R568

[22]. Xiangfeng Duan, Yu Huang, Ritesh Agarwal, and Charles M. Lieber, *Single-nanowire electrically driven lasers*, Nature 421, 241-245 (2003)

[23]. C. A. Stafford, *Metal Nanowires: Quantum Transport, Cohesion, and Stability*, Phys. Stat. Sol. (b) 230, No. 2, (2002) 481−489

[24]. S. Michotte, S. Matefi-Tempfli, and L. Piraux, *1D-transport properties of single superconducting lead nanowires*, Physica C 391 (2003) 369−375

[25]. Y. Arakawa, K. Furuya, S. Komiyama, and H. Nakashima, *Mesoscopic Physics and Electronics*, Berlin; Heidelberg; New York; Barcelona; Budapest; Hong Kong; Milan; Paris; Santa Clara; Singapore; Tokyo: Springer, (1998)

[26]. V. Rodrigues, J. Bettini, A. R. Rocha, L. G. C. Rego, and D. Ugarte, *Quantum conductance in silver nanowires: Correlation between atomic structure and transport properties*, Physical Review B, Vol. 65, 153402 (2002)

[27]. Richard L. Liboff, *Introductory Quantum Mechanics*, 4th edition, Addison Wesley, 2003

[28]. Igor Aharonovich, Shoshana Tamir, and Yeshayahu Lifshitz, *Growth of SiOx nanowires by laser ablation*, Nanotechnology 19 (2008) 065608

[29]. X.M. Cai , A.B. Djurišić, M.H. Xie, *GaN nanowires: CVD synthesis and properties*, Thin Solid Films 515 (2006) 984–989

[30]. Shi-biao Xiang, and Xu Xiang, *Novel 2D self-assembled arrays of SiOx nanowire bundles*, Materials Letters 61 (2007) 3662 – 3665

[31]. Yukihito Kondo, and Kunio Takayanagi, *Gold Nanobridge Stabilized by Surface Structure*, Phys. Rev. Lett., Vol. 79, No. 18, (1997) 3455-3458

[32]. Yukihito Kondo, and Kunio Takayanagi, *Synthesis and Characterization of Helical Multi-Shell Gold Nanowires*, Science, Vol. 289 No. 28 (2000) 606-608

[33]. Pablo Z. Coura, Sergio B. Legoas, Anderson S. Moreira, Fernando Sato, Varlei Rodrigues, Socrates O. Dantas, Daniel Ugarte, and Douglas S. Galvao, *On the Structural and Stability features of Linear Atomic Suspended Chains Formed from Gold Nanowires Stretching*, Nano Lett., Vol. 4, No. 7, (2004) 1187-1191

[34]. Yanfa Yan, Ping Liu, M. J. Romero, and M. M. Al-Jassim, Formation of metallic zinc nanowires, J. Appl. Phys., Vol. 93, No. 8, (2003) 4807-4809

[35]. Dmitri Routkevitch, Terry Bigioni, Martin Moskovits, and Jing Ming Xu, *Electrochemical Fabrication of CdS Nanowire Arrays in Porous Anodic Aluminum Oxide Templates*, J. Phys. Chem. (1996) 100, 14037-14047

[36]. A. J. Yin, J. Li, W. Jian, A. J. Bennett, and J. M. Xu, *Fabrication of highly ordered metallic nanowire arrays by electrodeposition*, Appl. Phys. Lett., Vol. 79, No. 7, (2001) 1039-1041

[37]. Massood Z. Atashbar, Deep Banerji, and Srikanth Singamaneni, *Room-Temperature Hydrogen Sensor Based on Palladium Nanowires*, IEEE Sensors Journal, Vol. 5, No. 5, (2005) 792-797

[38]. Erich C. Walter, Michael P. Zach, Fredric Favier, Benjamin J. Murray, Koji Inazu, John C. Hemminger, and Reginald M. Penner, *Metal Nanowire Arrays by Electrodeposition*, ChemPhysChem. (2003) 4, 131 – 138

[39]. E. J. Menke, M. A. Thompson, C. Xiang, L. C. Yang, and R. M. Penner, *Lithographically patterned nanowire electrodeposition*, Nature Materials, Vol. 5, (2006) 914-919

[40]. Milan Paunovic and Mordechay Schlesinger, *Fudanmentals of Electrochemical Deposition*, John Wiley & Sons, Inc., 1998.

[41]. NANO™ PMMA & Copolymer, Microchem Website, http://www.microchem.com/products/pdf/PMMA_Data_Sheet.pdf

[42]. Michael Kohler, and Wolfgang Fritzsche, *Nanotechnology*, WILEY-VCH Publishing, Weinheim, Germany, 2004

[43]. Andreas Mandelis and Jose A. Garcia, *Pd/PVDF thin film hydrogen sensor based on laser-amplitude-modulated optical-transmittance: dependence on H2 concentration and device physics*, Sensors and Actuators B 49 (1998) 258–267

[44]. Ted B. Flanagan and W. A. Oates, *The Palladium-Hydrogen System*, Annu. Rev. Mater. Sci. (1991) 21: 269-304

[45]. F. A. Lewis, *The Palladium Hydrogen System,* Academic Press, NY (1967).

[46]. J. C. Barton, F. A. Lewis, and (in part) Miss I. Woodward, *Hysteresis of the Relationships between Electrical Resistance and the Hydrogen Content of Palladium*, Trans. Faraday Soc. 59 (1963), p. 1201. **DOI:** 10.1039/TF9635901201

[47]. Yeonho Im, Choonsup Lee, Richard P. Vasquez, Mangesh A. Bangar, Nosang V. Myung, Eric J. Menke, Reginald M. Penner, and Minhee Yun, *Investigation of a Single Pd Nanowire for Use as a Hydrogen Sensor*, Small (2006) 2, No. 3, 356–358

[48]. T. A. Witten and L. M. Sander, *Diffusion-limited Aggregation*, Phys. Rev. B, Vol. 27, No. 9, (1983) 5686-5697

[49]. Fernando Patolsky, Brian P. Timko, Gengfeng Zheng, and Charles M. Lieber, *Nanowire-Based Nanoelectronic Devices in the Life Sciences*, MRS Bulletin, Vol. 32, (2007) 142-149

[50]. Manju Gerard, Asha Chaubey, and B.D. Malhotra, *Application of conducting polymers to biosensors*, Biosensors & Bioelectronics 17 (2002) 345–359

[51]. Kumaran Ramanathan, Mangesh A. Bangar, Minhee Yun, Wilfred Chen, Ashok Mulchandani, and Nosang V. Myung, *Individually Addressable Conducting Polymer Nanowires Array*, Nano Lett., Vol. 4, No. 7, (2004) 1237-1239

[52]. Yeonho Imb, Richard P. Vasquezc, Choonsup Leec, Nosang Myungd, Reginald Pennere, and Minhee Yun, *Single metal and conducting polymer nanowire sensors for chemical and DNA detections*, Journal of Physics: Conference Series 38 (2006) 61–64